



## Products of the iron cycle on the early Earth

Nicholas J. Tosca<sup>a,\*</sup>, Clancy Zhijian Jiang<sup>a</sup>, Birger Rasmussen<sup>b</sup>, Janet Muhling<sup>b</sup>

<sup>a</sup> Department of Earth Sciences, University of Oxford, South Parks Road, Oxford, OX1 3AN, UK

<sup>b</sup> School of Earth Sciences, The University of Western Australia, Perth, WA, 6009, Australia

### ABSTRACT

Traditional models for pre-GOE oceans commonly view iron as a critical link to multiple biogeochemical cycles, and an important source of electrons to primary producers. However, an accurate and detailed understanding of the ancient iron cycle has been limited by: (1) our ability to constrain primary depositional processes through observations of the ancient sedimentary rock record, and (2) a quantitative understanding of the aqueous geochemistry of ferrous iron. Recent advances in high resolution petrography and experimental geochemistry, however, have contributed to a new understanding of certain aspects of the early Fe cycle. Most importantly, high resolution petrographic studies of late Archean/early Paleoproterozoic iron formation have documented the prolific deposition of Fe(II)-silicate-rich chemical muds from a dominantly anoxic ocean. At the same time, recent experimental work has shed new light on processes likely to have controlled steady state Fe concentrations in Archean oceans. These studies suggest that spontaneous precipitation of Fe(II)-carbonate was probably rare in Archean oceans, and that Fe(II)-carbonate would have more commonly precipitated on the surfaces of suitable mineral substrates within clastic and chemical sediments, consistent with petrographic observations. In addition, although experimental investigations suggest that maximum Fe concentrations in Archean oceans would have been limited by authigenic Fe(II)-silicate production (rather than Fe(II)-carbonate), the rock record indicates that this process was rarely operative. Instead, sedimentology, stratigraphy, and geochemical modelling suggest that much of the precursor sediment to late Archean iron formation was produced as hydrothermal effluent interacted with seawater in close proximity to seafloor vents. Together, these observations help define a new topology for the ancient Fe cycle. In this view, hydrothermal effluent-seawater mixing would have strongly attenuated the flux of dissolved Fe<sup>2+</sup> to Archean oceans, and early diagenetic siderite formation may have balanced globally averaged riverine and hydrothermal Fe<sup>2+</sup> input fluxes. In contrast to previous models, this emerging picture of the early Fe cycle suggests that Fe played only a negligible role in supporting anoxygenic phototrophs, reinforcing the concept that electron donors were in comparatively limited supply before the advent of oxygenic photosynthesis.

### 1. Introduction

The evolution of oxygenic photosynthesis marks a crucial turning point in biology's evolutionary trajectory. Appreciating the full impact of this singular innovation on the ocean-atmosphere system requires that we understand how biogeochemical cycles were structured before, and after, its inception. Before the accumulation of O<sub>2</sub> in the oceans and atmosphere, iron assumed critical importance as a key electron donor on the early Earth [1–4]. Chemical interactions with SiO<sub>2</sub>(aq) and dissolved inorganic carbon, for example, would have driven mineral precipitation and thus regulated Fe concentrations in the early ocean, which may have controlled electron availability for early anoxygenic phototrophs, among other organisms, before the advent of oxygenic photosynthesis [5–8]. These interactions, in turn, may have strongly influenced the rates of primary productivity and the structure of the early carbon cycle, ultimately setting the stage for large-scale re-organisation after biology's greatest development.

Surprisingly, however, gaps still persist in our understanding of the pathways and products of Fe-based chemical sedimentation from early oceans. In part, these arise from two research challenges. The first

involves developing a more quantitative understanding of reaction rates and products involving ferrous iron and applying this understanding to aid in the interpretation of mineralogical, chemical, and isotopic signatures recovered from ancient rocks. Because these data were largely unavailable at the time, early views of the Fe cycle relied instead upon thermodynamic predictions of important reactions thought to have taken place in the water column or in sediment pore waters [5–8]. Together these calculations mark a critical starting point, and have shaped our current view of iron cycling on the early Earth. New experimental geochemical data, however, offer an opportunity to adapt these early models into a more quantitative framework. In fact, as we discuss below, many of the conclusions reached by earlier researchers, based on thermodynamic calculations, are compatible with newly available geochemical constraints. A second challenge arises from the fragmentary nature of the Archean sedimentary record, and the probability that ancient sedimentary successions have been metamorphosed or otherwise altered after deposition. Although chemical sediments are preserved in a number of Archean successions, their extensive post-depositional history commonly features multiple generations of diagenesis and/or mineral transformation. A correct interpretation of

\* Corresponding author.

E-mail address: [nick.tosca@earth.ox.ac.uk](mailto:nick.tosca@earth.ox.ac.uk) (N.J. Tosca).

<https://doi.org/10.1016/j.freeradbiomed.2019.05.005>

Received 1 December 2018; Received in revised form 18 April 2019; Accepted 2 May 2019

Available online 06 May 2019

0891-5849/ © 2019 The Authors. Published by Elsevier Inc. This is an open access article under the CC BY license (<http://creativecommons.org/licenses/by/4.0/>).

ancient sedimentary rocks therefore requires de-convolving primary (i.e., marine) mineral products from those that are largely post depositional in origin.

Over the last few years, a number of advances have been made on both of these fronts. For example, the application of new micro-analytical tools to ancient sedimentary rocks now allows geochemical signals to be imaged, at the micro- and nano-scale, in space and through time [9–13]. These data provide unique constraints on the mineral phases hosting geochemical signals and so underpin the successful development of new and existing palaeo-environmental proxies. At the same time, more kinetic and observational data from Fe(II)-bearing systems have become available over the last few years [14–17]. This has helped develop a more quantitative modelling of the early Fe cycle, and makes specific predictions for minerals that could be preserved in the sedimentary record.

Here we review the structure and dynamics of the early Fe cycle, with a focus on the late Archean as a prelude to the initial oxygenation of Earth's atmosphere. First, we highlight recent advances in interrogating the sedimentary record of Fe-rich rocks deposited before the great oxygenation event. We then review new constraints from experimental geochemistry that shed light on solubility-limiting reactions in dominantly anoxic Archean oceans. Finally, we combine these two sources of information to develop an emerging view of the Archean iron cycle that is consistent with both observations from sedimentary geology and inorganic geochemistry. We consider the implications of this view and highlight areas for future work.

### 1.1. The geochemistry of Archean seawater

An in-depth discussion of the geochemistry of Archean (4.0–2.5 Ga) oceans is provided by Halevy et al. in this issue. Here, we briefly touch upon two key aspects of Archean seawater chemistry of particular relevance to the ancient iron cycle.

Sedimentary rocks have long indicated that Archean seawater was chemically distinct from modern and geologically recent intervals (e.g. Refs. [6,18]). In particular, the sedimentary record indicates that Archean seawater featured significant concentrations of dissolved silica (expressed here as  $\text{SiO}_2(\text{aq})$ ) [19–24]. This is in sharp contrast with modern oceans, which, because of the extensive production of siliceous skeletons (i.e., diatoms, but also to a lesser extent radiolaria and sponges [25]), are relatively depleted in  $\text{SiO}_2(\text{aq})$ . Given that a biological silica sink would have been absent from Archean seawater, a logical inference is that abiotic reactions in sediment pore waters, or in the water column, would have controlled marine  $\text{SiO}_2(\text{aq})$  [19].

This reasoning is strongly supported by sedimentological and isotopic evidence. Although much of the sedimentary silica present in Archean rocks is late diagenetic in origin (i.e., replacing other lithologies after deposition [26,27]), a number of well-preserved examples show clear evidence for early diagenetic or even syndepositional precipitation of silica [20,22–24,28]. This style of precipitation is fundamentally distinct from younger siliceous sediments [20,29,30]. For example, the recognition of sand to silt-sized silica granules accumulating along sedimentary bedding planes provides compelling evidence that silica precipitated directly from Archean seawater [22,24]. Regular alternations of these beds with granule-poor and generally ferruginous chert suggests that the generation of silica granules was driven by periodic fluctuations in seawater chemistry [22,24]. Silica polymerization (the first step toward precipitation) from solutions of relatively high  $\text{SiO}_2(\text{aq})$  is sensitive to both pH and salinity [24,31,32]. On this basis, Stefurak et al. [24] logically reasoned that salinity fluctuations may have triggered silica granule formation, given the lack of obvious mechanisms that could have driven significant pH variations across continental shelf environments.

In addition to sedimentological data, the silicon isotopic composition of siliceous Precambrian (> 0.54 Ga) sedimentary rocks helps constrain the dominant silica sources to early oceans. These data

indicate that silica was supplied to Archean (4.0–2.5 Ga) and Palaeoproterozoic (2.5–1.6 Ga) seawater mainly through hydrothermal fluids, with continental silica fluxes becoming more important later in the Proterozoic Eon (defined as the interval spanning 2.5–0.54 Ga) [33,34]. Together, sedimentological and isotopic data suggest that Archean seawater was probably poised near the solubility limit of amorphous silica. In fact, marine  $\text{SiO}_2(\text{aq})$  concentrations may have, at times, exceeded this threshold if silica-rich granules identified by Stefurak et al. [24] formed through polymerisation of colloidal silica and particle aggregation [31,32].

Precambrian sedimentary rocks also reflect a  $\text{CaCO}_3$  cycle, and, by extension, marine carbonate chemistry, that differed markedly from younger geological intervals. Because Archean carbonates pre-date the advent of  $\text{CaCO}_3$ -based skeletonization, they are distinct from Phanerozoic counterparts; they are fundamentally the products of inorganic precipitation rather than skeletal production [35,36]. In addition, Archean carbonates reflect different styles of inorganic  $\text{CaCO}_3$  precipitation, even when compared to younger Proterozoic carbonates [35,36]. For example,  $\text{CaCO}_3$  was commonly precipitated directly on the Archean seafloor, as botryoidal fans of former aragonite and/or thick encrustations of calcite [36,37]. These characteristics are thought to reflect higher average seawater  $\text{CaCO}_3$  saturation state compared to modern oceans [38,39], or decreased gradients in  $\text{CaCO}_3$  saturation between surface seawater and the seafloor due to the effects of anoxic respiration [40]. Consistent with these suggestions, recent constraints on seawater carbonate chemistry, derived from the Ca isotopic composition of late Archean and early Proterozoic carbonate rocks, suggest that the dissolved inorganic carbon (DIC) pool was larger than today, approximately 2–20 mmol/kg, with atmospheric  $\text{CO}_2$  ranging from 10 to 100 times higher than modern values; these constraints correspond to seawater pH values of approximately 6.7–7.7 [41].

Together, chemical sediments deposited on late Archean continental shelves reflect seawater that commonly featured elevated concentrations of both  $\text{SiO}_2(\text{aq})$  and dissolved inorganic carbon. Given that soluble Fe may be readily precipitated in silicate or carbonate minerals, how would this have influenced marine Fe concentrations? How might these processes be expressed in ancient sedimentary rocks? The sedimentary record of iron-rich rocks provides answers to these questions, with the caveat that appropriate care must be taken to deconvolve primary or syndepositional mineral products from those that are post depositional in origin.

## 2. Constraints on the early Fe cycle from iron formation

### 2.1. Traditional models

Archean sedimentary rocks, long recognised by geologists as conspicuously enriched in iron, offer an unusually accessible record of the early iron cycle. Several workers have emphasised compositional differences between Archean and post-Archean clastic sedimentary rocks [42–44], but Kump and Holland (1992) [45] further examined secular patterns in Fe enrichment. They showed that Fe was added to marine siliciclastic sediments at a flux (relative to the total deposition rate) that increased the average bulk Fe content by a factor of two compared to younger equivalents. How, and in what form (i.e., particulate or dissolved) was this Fe delivered to Archean marine sediments? Although clastic sedimentary rocks provide clear evidence for secular change in bulk Fe enrichment, chemically-precipitated sedimentary rocks have yielded the most important constraints on Fe delivery mechanisms. In particular, iron formation, a chemical sedimentary rock deposited through much of the Archean (and specific intervals at the beginning and end of the Proterozoic [46]), serves as our most important archive of the processes that removed iron from seawater and the mineral products that entered precursor sediments.

Early models for the origin of iron formation centred mainly on the origin of hematite ( $\text{Fe}_2\text{O}_3$ ), the oxidised Fe-mineral principally

responsible for imparting the distinctive red colour to many (but not all) of the most iconic deposits (i.e. [47]). Depositional and diagenetic models have long hypothesised that the finest-grained (or “dusty”) hematite, commonly trapped in early diagenetic chert, might represent minerals formed directly from seawater [48–52]. This inference, based predominantly on small particle size (i.e., following criteria established by Ref. [53]), along with thermodynamic calculations that appeared to reconcile the co-existence of hematite, siderite ( $\text{Fe}^{\text{II}}\text{CO}_3$ ), and pyrite ( $\text{Fe}^{\text{II}}\text{S}_2$ ) in modern and ancient sediments [54], led to a general acceptance that the dusty hematite represented a primary precipitate from Archean seawater (see Ref. [55] for historical context). This, in turn, prompted models for the origin of hematite through oxidation of soluble  $\text{Fe}^{2+}$  via iron-oxidising photosynthesis or reaction with  $\text{O}_2(\text{aq})$  produced from cyanobacteria (first suggested by Ref. [56]). Other ideas for the origin of oxidised Fe-phases in iron formation included UV photolysis [57], though Konhauser et al., 2007 [58] later suggested that photolysis rates were probably too slow to account for apparent depositional rates of iron formation.

As a consequence, genetic models for iron formation, developed over the last several decades, have posited that much of the hematite was derived from the dehydration of Fe(III)-oxides that initially entered iron formation precursor sediments [48–52,59]. This oxidised Fe is generally hypothesised to have served as a source of electron acceptors for dissimilatory iron reduction during early diagenesis [60,61]. In this view, reduced Fe(II)-bearing phases would be predominantly diagenetic in origin, formed through the re-reduction of Fe in combination with various dissolved pore water components to generate magnetite ( $\text{Fe}^{\text{II}}|\text{Fe}^{\text{III}}\text{O}_4$ ), siderite, and Fe(II)-silicates [60]. A supporting line of evidence for this hypothesis comes from the negative carbon isotopic composition (expressed as  $\delta^{13}\text{C}$ ) of many iron formation carbonates, which was originally suggested to reflect the influence of microbial iron reduction coupled to organic matter oxidation [60]. More recent isotopic investigations have inferred that such processes may also be recorded by iron isotopes because iron formation carbonates and magnetite feature depleted  $\delta^{56}\text{Fe}$  values that correlate with negative  $\delta^{13}\text{C}$  [62–65].

## 2.2. New constraints on the origin of late Archean/early Palaeoproterozoic iron formation

Given that traditional optical microscopy was the principal tool available to early investigators of iron formation, the advent of high-resolution electron microscopy has increased the effective spatial resolution at which observations can be made by 4 orders of magnitude. This has offered a new opportunity to re-examine iron formation successions and re-assess paragenetic relationships between minerals. With this goal in mind, Rasmussen and colleagues, in a series of recent studies, applied a combination of transmission/reflected light microscopy, backscattered electron imaging, and high angle annular dark-field STEM and TEM microscopy on focused ion beam (FIB)-milled specimens of iron formation [11,21,55,66,67]. The examination of several hundred thin sections, sampled from well-preserved drill core through the 2.63–2.45 Ga Hamersley Group, Australia, led Rasmussen et al. [11,55,67] to conclude that much of the finest-grained (so called “dusty”) hematite is consistent with a secondary, or post-depositional, origin. This conclusion is supported by the following groups of observations (Fig. 1):

1. Hematite dust is concentrated along grain boundaries, cleavage planes and within altered grains of diagenetic/metamorphic Fe(II)-carbonates and Fe(II)-silicates.
2. Transition zones from green to red chert are commonly observed along individual sedimentary laminae; these are discordant to sedimentary bedding. These observations are not immediately compatible with hypotheses arguing for the precipitation of both Fe(II)-silicates (primarily responsible for green pigmentation) and Fe(III)-

oxide/hydroxides (responsible for red/orange pigmentation) from the same water column.

3. Replacement of Fe(II)-silicate by hematite is commonly observed along hairline fractures that cross-cut laminated chert.
4. Cavities are commonly observed to contain Fe(II)-silicate which sometimes occurs with hematite in the same cavity. These cavities are inferred to represent dissolution/precipitation processes associated with mineral replacement reactions that created nano-pore space eventually filled or replaced by hematite.
5. Relict Fe(II)-silicate nanoparticles are abundant and commonly found preserved in otherwise red cherts.

Perhaps the most important conclusion drawn from high-resolution petrographic studies of Archean iron formation is that the mineral phases displaying the clearest evidence for a primary origin are Fe(II)-silicates, specifically greenalite ( $\text{Fe}_3\text{Si}_2\text{O}_5(\text{OH})_4$ ) and possibly stilpnomelane ( $(\text{K,Ca,Na})(\text{Fe,Mg,Al})_8(\text{Si,Al})_{12}(\text{O,OH})_{36}\cdot n\text{H}_2\text{O}$ ) [11,21,55,66,67]. A primary origin is supported by pervasive Fe(II)-silicate nanoparticles trapped in early diagenetic chert (Fig. 2), formed via silicification at or below the seafloor during or shortly after the re-working and accumulation of Fe(II)-silicate muds [11,21,55,66,67]. In fact, sedimentological and petrographic evidence of silica-rich horizons in Archean iron formation that show that silicified Fe(II)-bearing muds were subsequently re-worked into intraformational sandstones, indicating that Fe(II)-silicate deposition and silicification occurred syndepositionally (i.e. [28]). More recent investigations of iron formation successions from the late Archean Transvaal Supergroup lead to a similar conclusion. Here, Fe(II)-silicates appear to represent the dominant depositional phase, also commonly preserved in chert [11]. Like the Hamersley Group, Fe(II)-silicate-rich horizons of iron formation in the Transvaal Supergroup are commonly replaced by coarser grained Fe(III)-oxide, Fe-silicate (i.e., minnesotaite) and Fe-carbonate minerals [11].

These high resolution petrographic and microscopic investigations have also shown that magnetite, a common mineral in nearly all Archean iron formation deposits, may also owe its origins to secondary replacement processes [68] (Fig. 3). Rasmussen and Muhling (2018) [68], focusing again on Hamersley Group iron formation, reached this conclusion based on the following groups of observations:

1. The identification of lateral transitions from siderite-rich Fe(II)-silicate bands into magnetite-rich bands.
2. Minute magnetite (and hematite) crystals along corroded grain boundaries and within partially altered grains of Fe(II)-carbonates and silicates. This suggests that dissolution-reprecipitation reactions were the dominant emplacement mechanism.
3. The association of magnetite with minute hematite particles surrounding altered mineral grains.
4. The development of scalloped and irregular boundaries between magnetite and reacting minerals such as ankerite and siderite. In these cases, magnetite also contains siderite and/or ankerite inclusions, consistent with a secondary origin.
5. Dissolution pits and cavities in siderite crystals adjacent to replacive magnetite.
6. Magnetite precipitation post-dates differential compaction, suggesting replacement occurred after significant burial and the establishment of overburden.

New observational constraints on the origin of magnetite in these deposits support two major conclusions. The first is that magnetite is dominantly replacive in Hamersley Group iron formation, and, given its close spatial association with siderite, likely originated through thermal decomposition reactions upon burial and metamorphism [68]. For example, experimental studies on the thermal decomposition of siderite have shown that in the presence of water, siderite breaks down to form magnetite, liberating  $\text{CO}_2$  and  $\text{H}_2$  in the process [69]. This occurs at temperatures  $\sim 200\text{--}350^\circ\text{C}$ , which corresponds to metamorphic



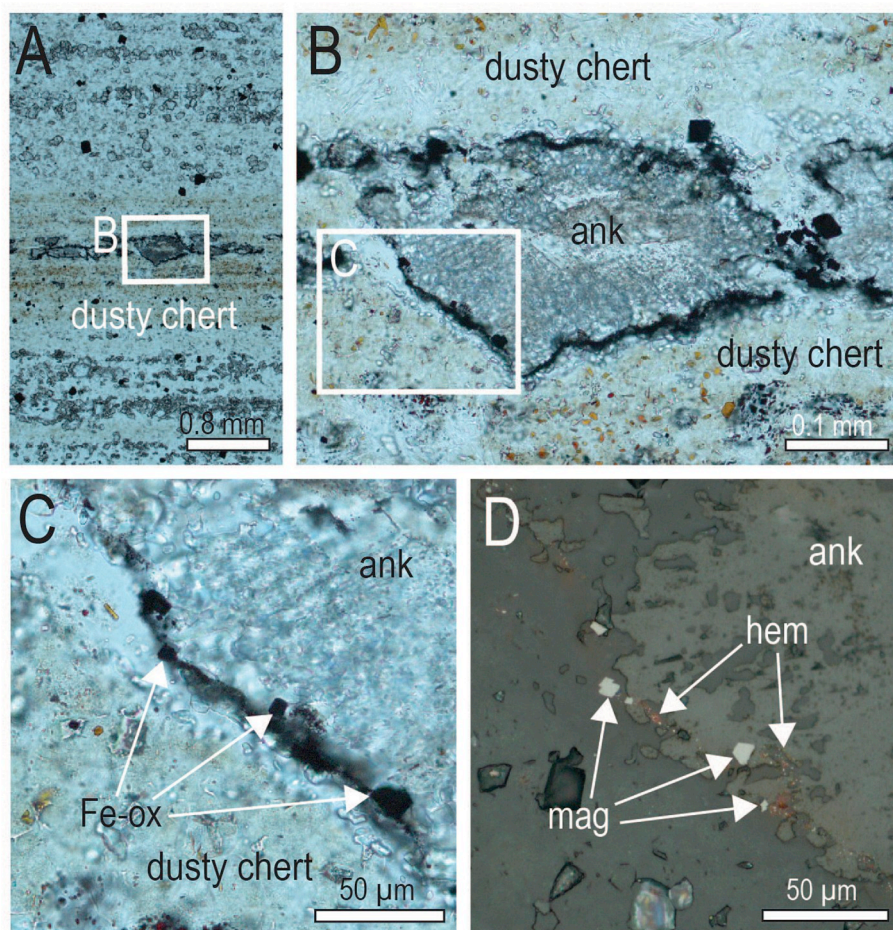


**Fig. 1.** Examples of post-depositional alteration and generation of fine-grained secondary hematite. Drill-hole ABDP9, 222.1–0.19 m (Mt Sylvia Formation, Hamersley Group). A and B. Transmitted light images of diagenetic ankerite (ank) in dusty chert. C. Transmitted light image of fine-grained magnetite and hematite (Fe-ox) concentrated at the edges of coarse-grained diagenetic ankerite. D. Reflected light image of fine-grained magnetite (mag) and hematite (hem) concentrated at the edges of coarse-grained diagenetic ankerite.

temperatures experienced by much of the Hamersley Group [68]. The second conclusion is that siderite appears to have commonly precipitated in, and/or along the surfaces of, greenalite-rich laminae before significant compaction took place, pointing to a dominantly early diagenetic origin [68].

### 2.3. A new depositional and diagenetic model for Archean iron formation

Together, the observations summarised above tightly constrain the principal depositional and diagenetic processes that generated late Archean and Palaeoproterozoic iron formation as well as their relative timing. As summarised by Rasmussen and Muhling (2018) [68], these processes commenced with prolific deposition of Fe(II)-silicate-rich muds (Fig. 4a). These highly porous muds were commonly silicified on the seafloor before compaction (Fig. 4b), yielding well-preserved greenalite nanoparticles trapped in chert (commonly referred to as “dusty chert”), and non-silicified greenalite-rich sediments. The precipitation of siderite on the surfaces of, and within, Fe(II)-silicate-rich laminae commonly occurred soon after initial deposition but, in many cases, before significant compaction [68] (Fig. 4c). Post-depositional transformation of siderite to fabric-destructive and/or replacive magnetite yields variably magnetite-enriched intervals among silicified sediments (Fig. 4d). Together, Fe(II)-silicate precipitation, in combination with variable amounts of seafloor silicification, were likely instrumental in generating alternating bands of silica-rich and iron-rich composition [11]. Post depositional interaction with repeated

generations of fluid flow linked to the ca. 2.2 Ga collision or accretion of the Glenburgh Terrane with the Pilbara Craton, known as the Ophthalmian Orogeny, would have driven the secondary formation of hematite (i.e. [67]), consistent with independent geochemical evidence for the appearance of oxygen-rich groundwaters during and shortly after the great oxidation event (i.e. [71]). Post-depositional deformation and fluid flow would also have promoted siderite replacement by magnetite via thermal decomposition.

These observations in turn invite new models for how the dominant mineralogical building blocks of iron formation, the Fe(II)-silicates, were initially precipitated. Rasmussen et al. [11], for example, suggested that mixing between hydrothermal effluent and ambient seawater might have triggered the precipitation of Fe(II)-silicate. This hypothesis finds support from sedimentological and stratigraphic studies indicating that iron formation intervals of the Hamersley Group are best interpreted as re-worked chemical sediments deposited on the flanks of submarine volcanoes rather than pelagites derived from chemical sedimentation from the water column [70]. In this model, the physical and chemical interaction of two fundamentally different fluid types would have modified local water column chemistry, commonly triggering the deposition of Fe(II)-silicate-rich muds. This process is returned to in more detail below.

The model proposed by Rasmussen et al. [11] contrasts markedly with previous models for the origin of iron formation in that dissolved oxygen is not required at the time of iron formation deposition. By extension, the role of anoxygenic photosynthesis in generating a flux of



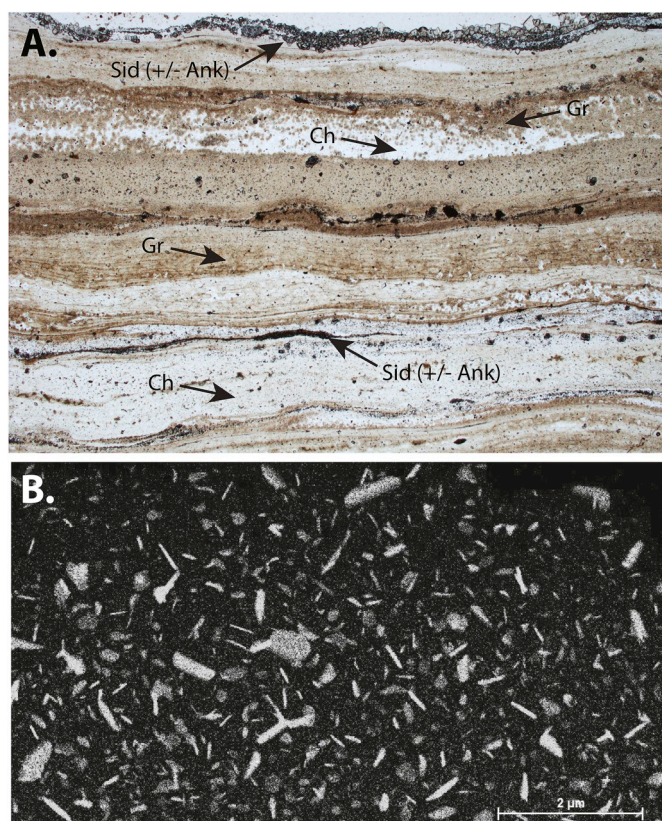


**Fig. 2.** A. Greenalite-rich laminae and chert (Drill hole ABDP9, 288.23–0.36 m (Wittenoom Formation, Hamersley Group). Ch = chert; Sid = siderite; Ank = ankerite; Gr = greenalite. B. Transmission electron microscopy image of greenalite nanoparticles trapped in chert (Drill hole ABDP9, 37 m).

oxidised iron to precursor sediments is not easily reconciled with the observations outlined above, or with new micro-analytical constraints indicating that greenalite preserved in iron formation chert contains little structural Fe(III) [12]. In addition, a dominantly post-depositional origin for magnetite suggests that the involvement of microbial processes in modifying initial iron formation mineral assemblages during early diagenesis may not be as clearly recorded in these successions as previously thought [68].

The new model advocated by Rasmussen et al. [11] also raises a number of questions regarding the early iron cycle and how it was structured before the GOE. Specifically, if Fe(II)-silicate minerals were indeed the primary building blocks of late Archean/early Palaeoproterozoic iron formation successions, what processes triggered their precipitation, and how might this have influenced marine  $\text{Fe}^{2+}$  concentrations? Similarly, what processes triggered early diagenetic siderite precipitation in iron formation sediments, and why, in many instances, was it concentrated along Fe(II)-silicate-rich laminae? More broadly, how do these deposits constrain the nature of chemical interactions between  $\text{Fe}^{2+}$ ,  $\text{SiO}_2(\text{aq})$ , and dissolved inorganic carbon?

### 3. Inorganic controls on the early Fe cycle: experimental constraints

A quantitative interpretation of the ancient rock record requires an understanding of the rates and processes of Fe-mineral precipitation from early oceans. Over sufficiently long timescales, Fe(II)-mineral precipitation must have balanced hydrothermal and continental delivery of  $\text{Fe}^{2+}$  to early oceans. Available constraints indicate that dissolved inorganic carbon and  $\text{SiO}_2(\text{aq})$  were abundant in Archean oceans. Thus, from first principles, mineral sinks that would have controlled  $\text{Fe}^{2+}$  availability should be dominated by three processes: Fe(II)-silicate precipitation, Fe(II)-carbonate precipitation, and green rust precipitation. Although quantitative data with which to interpret Fe-mineral precipitation from such systems has been lacking, recent experimental studies have clarified all three of these processes with a specific focus on the ancient iron cycle.

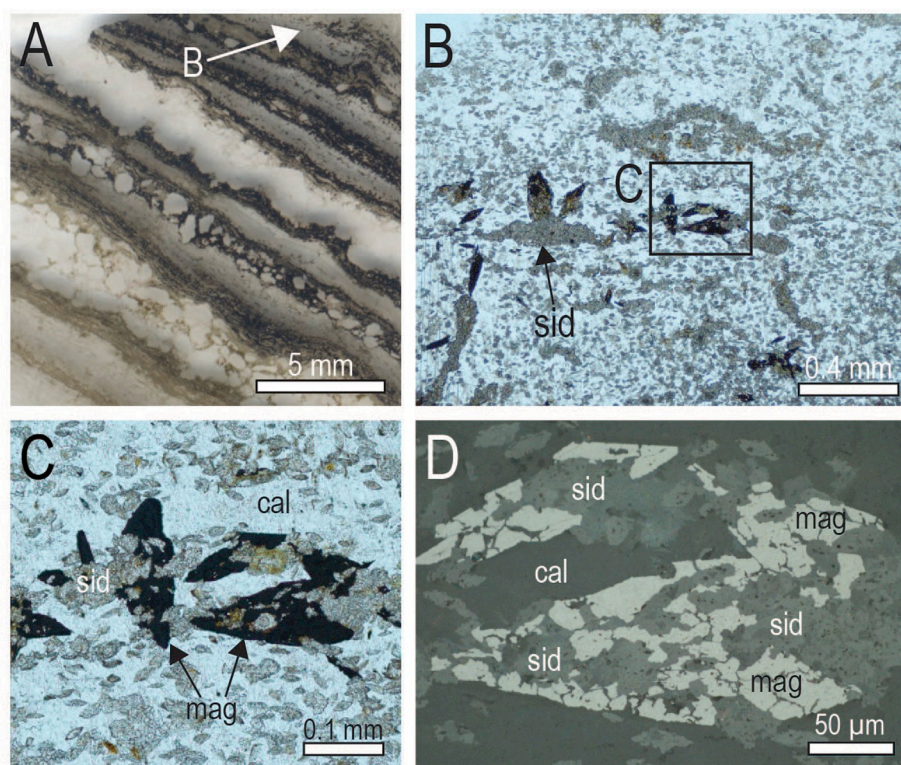


**Fig. 3.** Examples of post-depositional alteration and oxidation of siderite. Drill-hole Mitchell-2, 311.0 m (Dales Gorge Member, Brockman Iron Formation, Hamersley Group). A-C. Transmitted light images of laminated Fe-oxides and chert. D. Reflected light image of alteration textures of magnetite overgrowths including and overprinting finely crystalline siderite with coarser, crystalline fabric.

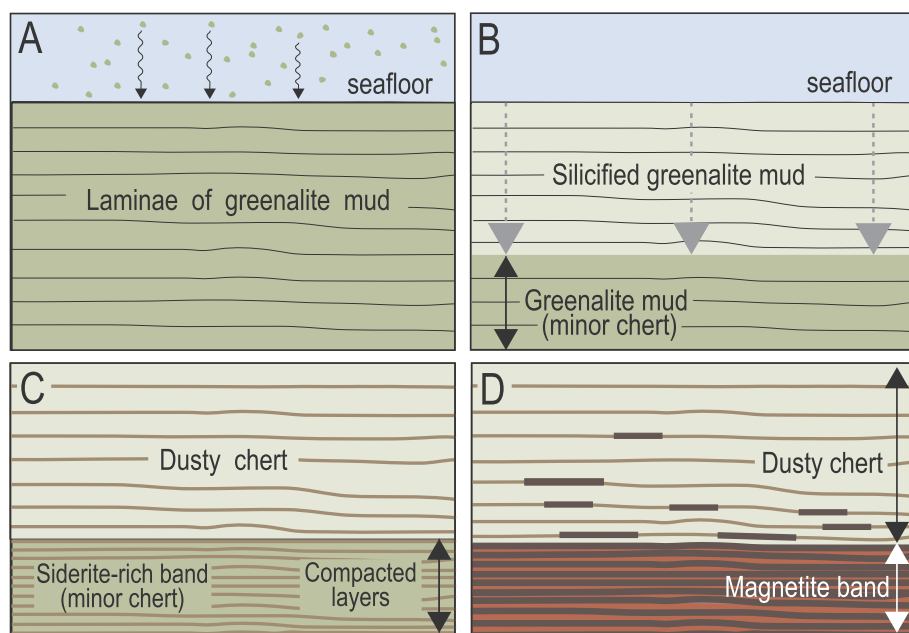


**Fig. 4.** Schematic diagram for the formation of magnetite-rich bands in Hamersley Group iron formation [68]. A. Precipitation of greenalite nanoparticles and micro-granules in the water column, forming laminae of porous, greenalite mud. B. Silica cementation of greenalite mud prior to compaction forming tabular beds. C. Compaction of non-silicified greenalite mud. Growth of siderite in greenalite mud and along laminae surfaces. D. Replacement of siderite and greenalite in compacted iron-rich bands by magnetite and hematite during fluid alteration.

### 3.1. The Fe(II)–SiO<sub>2</sub>(aq) system

The pre-GOE sedimentary record abounds with evidence indicating that seawater was enriched in SiO<sub>2</sub>(aq), persistently anoxic, and at times, ferruginous. Under what conditions might Fe<sup>2+</sup> and SiO<sub>2</sub>(aq) interact with one another? In conducting a series of closed system anoxic precipitation experiments, Tosca et al. (2016) [15] observed that, over a wide range of conditions, Fe<sup>2+</sup> and SiO<sub>2</sub>(aq) concentrations in synthetic seawater were limited by the precipitation of poorly crystalline Fe(II)-silicate. These results suggest that Fe(II)-silicate precipitation may have played a role in controlling Fe<sup>2+</sup> concentrations of the early oceans.

Using powder X-ray diffraction, FT-IR spectroscopy, thermo-gravimetric analysis, and TEM, Tosca et al. (2016) [15] showed that the synthetic material exhibited close structural similarities with the mineral greenalite, commonly observed in Archean iron formation (i.e. [11,21,66,72]). For example, absorption features present in FT-IR spectra corresponded closely to those observed for natural greenalite, indicating that although the material was poorly crystalline, it featured nearly identical structural characteristics (i.e., a trioctahedral layer occupied by Fe(II) and the attachment of that layer, at least at the local scale, to silica tetrahedra) [15]. TEM data also identified the presence of nano-crystalline domains within the hydrous Fe(II)-silicate precursor, which implied that incipient dehydration and rearrangement of the structure (thermodynamically favoured but kinetically slow) had begun during the experiments.

Given the close correspondence between the experimentally produced solids and natural greenalite, Tosca et al. (2016) [15] suggested that greenalite could be readily precipitated from Archean seawater at ambient temperature (25 °C). They suggested that such a process would be initiated by the nucleation of a poorly crystalline Fe(II)-silicate precursor directly from solution (which we refer to as homogeneous nucleation) and structural re-arrangement to greenalite. By extension, Tosca et al. (2016) concluded that the solubility of the Fe(II)-silicate precursor itself may have exerted an important control on Fe concentrations in the pre-GOE ocean.

Experiments conducted by Tosca et al. (2016) [15] revealed that a supersaturation threshold must be crossed in order for the Fe(II)-silicate precursor to form directly from water (Fig. 5). At or above this level of supersaturation, nucleation from solution was observed; below this, Fe<sup>2+</sup> and SiO<sub>2</sub>(aq)-bearing seawater solutions apparently persisted in a

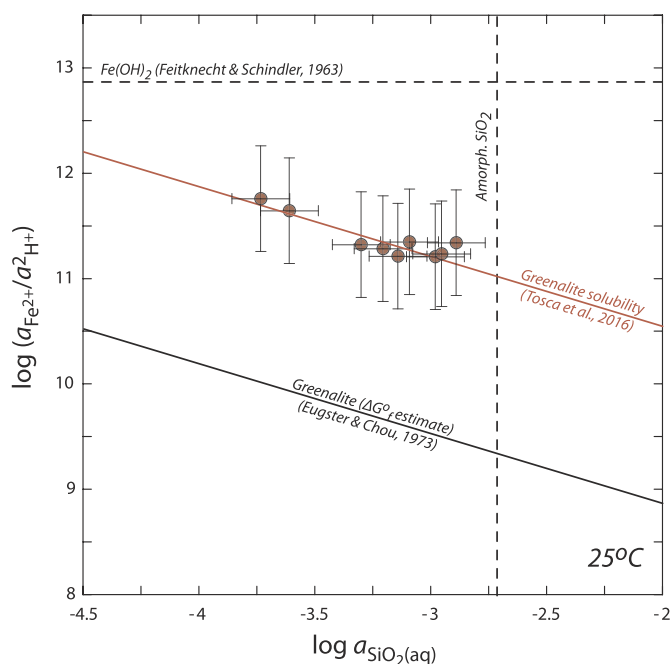


**Fig. 5.** Solubility diagram for the Fe<sup>2+</sup>-SiO<sub>2</sub>-H<sub>2</sub>O system at 25 °C. Increases in pH and/or Fe<sup>2+</sup> result in higher y-axis values, and increases in SiO<sub>2</sub>(aq) result in higher x-axis values. Dashed lines include solubility limiting phases: amorphous silica [115] and freshly precipitated Fe(OH)<sub>2</sub> [116]. Solid line corresponds to previously estimated greenalite solubility [7]. Final solution compositions are plotted as filled circles, corresponding to the apparent solubility of greenalite derived from experimental data. From Tosca et al. (2016).

metastable state with no detectable nucleation. The observation of a critical supersaturation is easier to understand in the context of nucleation rate theory. The experimental data produced by Tosca et al. (2016) [15] show that the instantaneous Fe(II)-silicate precursor precipitation rate exhibits a strong exponential dependence on supersaturation (with respect to greenalite) (Fig. 6). Because precipitation phenomena observed by Tosca et al. (2016) [15] were dominated by nucleation rather than growth (i.e., generating many small particles rather than fewer larger ones), the data can be well explained with a



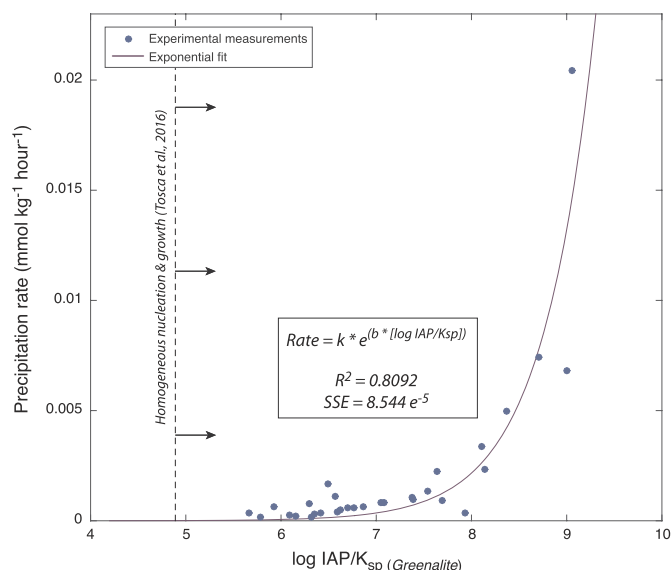


**Fig. 6.** Experimentally determined greenalite precipitation rate as a function of supersaturation. Data points represent experimental measurements of greenalite precipitation rate by Tosca et al. (2016). These data define a relationship identical in form to nucleation rates predicted by kinetic theory.

general expression for the nucleation rate of a solid substance from water derived from classical nucleation theory [73,74]. This expression predicts that, because of the strong exponential dependence of Fe(II)-silicate nucleation rate on supersaturation, precipitation rates are prohibitively slow at values less than the apparent threshold; so slow that observable increments of greenalite precipitation exceed reasonable early diagenetic timescales.

On the basis of their experimental measurements, Tosca et al. (2016) proposed that the formation and stability of the Fe(II)-silicate precursor should be dictated by specific combinations of pH,  $\text{SiO}_2(\text{aq})$ , and/or  $\text{Fe}^{2+}$  concentrations. For example, by expressing the apparent solubility of the Fe(II)-silicate precursor in terms of pH, Tosca et al. (2016) showed that for previous estimates of  $\text{Fe}^{2+}$  concentrations in the pre-GOE ocean ( $\sim 10\text{--}120\ \mu\text{mol/kg}$ , which were originally based on the assumption of siderite equilibrium solubility, discussed in more detail

below), and the assumption that  $\text{SiO}_2(\text{aq})$  values were poised at amorphous silica saturation, nucleation of Fe(II)-silicate from Archean seawater would have required a pH of  $\sim 7.7\text{--}8.3$ . These values are higher than recent model estimates of the pH of late Archean/early Palaeoproterozoic seawater, which place the expected pH between 6.3 and 7.7 [41,75,76]. Alternatively, if Fe(II)-silicate was the solubility-limiting phase precipitating from Archean seawater, and pH levels were instead between 6.3 and 7.7,  $\text{Fe}^{2+}$  concentrations in the pre-GOE oceans could have been about an order of magnitude higher than previously estimated. It is worth noting that the relationship displayed on Fig. 6, based on laboratory measurements, indicates that at pH below  $\sim 7.2$ , greenalite nucleation rates may have been too slow to exert strong control on Fe concentrations of Precambrian oceans.

Together, experimental data reported by Tosca et al. (2016) underscore that the precipitation of greenalite from Archean seawater could have been likely across a wide range of chemical conditions at relatively low temperatures. In addition, these results suggest that greenalite may have acted as the major solubility-limiting precipitate in Archean seawater, in turn exerting a strong upper limit on seawater  $\text{Fe}^{2+}$  concentrations. However, this latter conclusion is contingent on understanding the behaviour of the Fe(II)-carbonate system, which would have acted as another major control on  $\text{Fe}^{2+}$  concentrations in ferruginous non-sulfidic marine systems commonly envisaged for the Archean.

### 3.2. The Fe(II)-DIC-( $\text{SiO}_2(\text{aq})$ ) system

The sedimentary record of Precambrian carbonate rocks indicates that Archean seawater featured a larger DIC pool than the modern ocean (i.e. [41]). This implies that anoxic and ferruginous conditions may have commonly led to the precipitation of Fe(II)-carbonate minerals which, along with Fe(II)-silicates, may have acted as yet another important sink for  $\text{Fe}^{2+}$  in Archean systems. Although thermodynamic data have supported the long-held assumption that seawater would have been poised at siderite and calcite saturation (i.e. [5,6]), few kinetic studies have investigated the rates and processes of Fe(II)-carbonate precipitation from ancient seawater.

In an effort to re-examine the role of Fe(II)-carbonate precipitation in the early iron cycle, Jiang & Tosca (2019) [17] investigated the precipitation kinetics of Fe(II)-carbonate in the presence and absence of

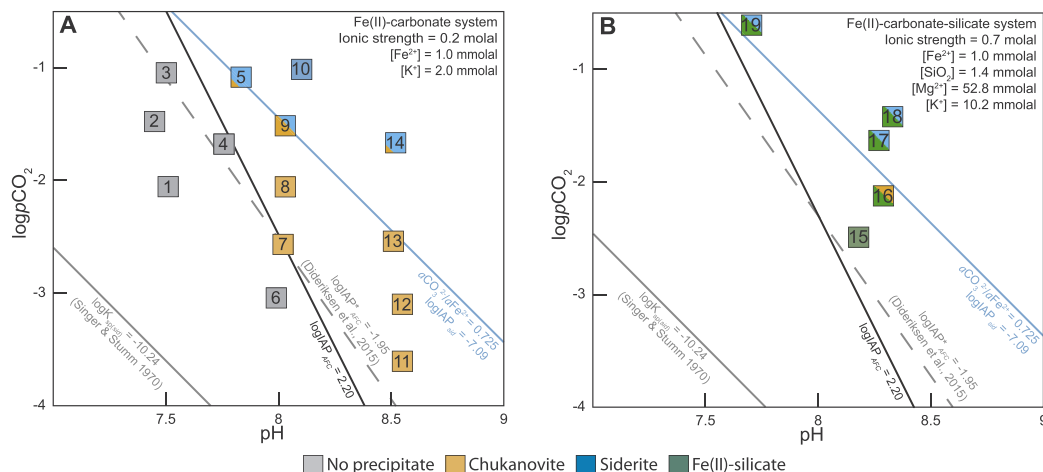


**Fig. 7.** Log  $p\text{CO}_2$ -pH plot of Fe(II)-carbonate precipitation experiments. (A). Fe(II)-carbonate system and (B). Fe(II)-carbonate-silicate system, with their corresponding chemical compositions. Overall, homogeneous nucleation of different Fe(II)-carbonate phases only occurred at high supersaturation (high log  $p\text{CO}_2$  and pH); critical supersaturation threshold for nucleation are placed where the corresponding mineral was identified from the experiment with the lowest initial saturation index: amorphous Fe carbonate  $\log \text{IAP}_{\text{AFC}} = -4.40$  (black solid line); siderite  $\log \text{IAP}_{\text{sid}} = -7.09$  (blue solid line). Siderite solubility  $\log K_{\text{sp}}(\text{sid}) = -10.24$  (grey solid line [117]) and AFC composition reported by Ref. [77] ( $\text{Fe}(\text{CO}_3)_{0.7}(\text{OH})_{0.6}$ ;  $\log \text{IAP}_{\text{AFC}} = -1.95$ ; grey dashed line) are plotted here for reference. From Jiang & Tosca (2019).

$\text{SiO}_2(\text{aq})$ . These experiments showed that spontaneous precipitation of Fe(II)-carbonate from anoxic, low  $\text{SO}_4$  seawater commonly results in a multi-step precipitation pathway that ultimately yields chukanovite ( $\text{Fe}_2^{II}(\text{CO}_3)(\text{OH})_2$ ) and/or siderite (Fig. 7). However, in the presence of  $\text{SiO}_2(\text{aq})$ , an Fe(II)-silicate precursor identical to that reported in Tosca et al. (2016) precipitated, despite relatively high  $p\text{CO}_2$  and pH (and therefore supersaturation with respect to Fe(II)-carbonate). An obvious question arises - which mineral would have been more important as a sink for  $\text{Fe}^{2+}$ , Fe(II)-carbonate or Fe(II)-silicate?

Jiang & Tosca's (2019) [17] experiments show that the spontaneous precipitation of Fe(II)-carbonate from anoxic seawater is strongly inhibited by kinetic processes. In fact, the supersaturation threshold for the nucleation of Fe(II)-carbonate from solution is similar in magnitude to that required to precipitate amorphous iron(II) carbonate (AFC), suggesting that AFC acts as a precursor for Fe(II)-carbonate precipitation from Archean seawater solutions. A potential role for AFC as a precursor for Fe(II)-carbonate is also consistent with SEM evidence showing unstable spherical precipitates displaying no obvious crystalline morphology at a scale of 10's of nm [17]. Indeed, all of the crystalline products produced from Jiang & Tosca's (2019) experiments displayed spherical morphology and evidence for recrystallisation from a precursor, consistent with observations of AFC synthesis and recrystallisation by Dideriksen et al. (2015) [77]. Jiang & Tosca (2019) concluded that the formation of AFC offered an energetically favourable route for precipitation whereby AFC provided reactive surface area to promote the secondary nucleation of crystalline materials (i.e., chukanovite and siderite), similar to what has been observed for the  $\text{CaCO}_3$  system [78].

Analogous to Fe(II)-silicate nucleation, the relationship between instantaneous Fe(II)-carbonate precipitation rate and supersaturation shows a strong exponential dependence, consistent with kinetic theory [17]. This again provides support for why an apparent critical supersaturation for Fe(II)-carbonate might have existed in Archean seawater, and offers insight into why many natural aquatic systems are often poised at relatively high supersaturation relative to siderite (i.e. [79,80]).

With an improved mechanistic understanding of Fe(II)-carbonate precipitation, Jiang & Tosca (2019) used their observations to address the question of whether Fe(II)-carbonate or Fe(II)-silicate was the more important sink for  $\text{Fe}^{2+}$  in Archean systems. By assuming that  $\text{Fe}^{2+}$  concentrations were controlled by the precipitation of Fe(II)-silicate (consistent with experimental observations), Jiang & Tosca (2019) evaluated the conditions required to trigger spontaneous precipitation of Fe(II)-carbonate from anoxic seawater over a finite range in pH (Fig. 8). The calculations show that significant supersaturation with respect to Fe(II)-carbonate is required - this corresponds to  $p\text{CO}_2$  and DIC concentrations far higher than any reasonable reconstruction of Precambrian seawater carbonate chemistry allows (i.e., from Ca isotopic composition of Precambrian carbonates [41]). A high supersaturation required for the nucleation of Fe(II)-carbonate is also consistent with a thermodynamic analysis of the solid solution compositions of Fe(II)-rich carbonates deposited in the Marra Mamba iron formation [81]. Woods & Garrels (1992) [81] concluded that the aqueous fluids assumed to have reached equilibrium with microcrystalline carbonate minerals of the Marra Mamba require much higher  $a_{\text{Fe}^{2+}}/a_{\text{Ca}^{2+}}$  ratios than reasonable estimates for Archean seawater.

Together, these results allow two conclusions which inform the nature of the early iron cycle. The first is that experimental constraints on nucleation kinetics show that the solubility-limiting phase in the Archean water column was very likely Fe(II)-silicate (eventually transforming to greenalite), not Fe(II)-carbonate. The second conclusion is that the origin of siderite in many iron formation successions either reflects: (1) the heterogeneous precipitation of Fe(II)-carbonate on pre-existing material surfaces, or (2) an origin that is distinct from seawater in equilibrium with ocean-atmosphere carbonate chemistry as

it is currently understood for the Archean (a conclusion in line with Woods & Garrels (1992) [81]).

### 3.3. Green rusts

Aside from Fe(II)-silicate and Fe(II)-carbonate, green rusts, a class of mixed valence Fe-rich double layer hydroxides, represent a third potentially important sink for  $\text{Fe}^{2+}$  in ferruginous non-sulfidic systems. On the basis of thermodynamic evidence, Halevy et al. (2017) [14] suggested that green rust may represent an important sink for Fe in Precambrian depositional systems and may have acted as a reactive intermediate responsible for generating multiple minerals observed in iron formation deposits. To examine this hypothesis, the authors conducted an experimental investigation based on a two-stage approach: (1) synthesis of green rust, and (2) ageing of green rust in aqueous media in the presence of  $\text{SiO}_2(\text{aq})$  and dissolved inorganic carbon. In investigating the first process, Halevy et al. (2017) observed that the exposure of anoxic  $\text{Fe}^{2+}$ -bearing seawater-type solutions to a slow diffusive flux of  $\text{O}_2(\text{g})$  resulted in the relatively rapid precipitation of green rust. Ageing the precipitates in various solutions (simulating the settling of green rust particles from the surface ocean to deeper anoxic waters) resulted in the recrystallisation of green rust into a variety of mineral phases depending on the chemistry of the ageing solution (for example, pH,  $\text{SiO}_2(\text{aq})$  and DIC concentration). The resultant precipitates included mixtures of siderite, magnetite, and various Fe-bearing silicates. To further examine the importance to global geochemical cycles, Halevy et al. (2017) constructed a time-resolved model for the early Fe cycle to explore the potential role of green rust as a major sink for Fe. The modelling results show that green rust may have been important at a global scale, dependent on the chemistry of seawater and the relative stability of other Fe-bearing phases.

In addition to the oxidative pathway envisaged by Halevy et al. (2017) for green rust formation, strictly anoxic pathways for precipitating green rust are possible, and these may in fact be applicable to Archean systems. For example, Tosca et al. (2018) [82] examined the evolution of pore water chemistry during the deposition and anoxic diagenesis of the Murray Formation, part of an ancient fluvio-lacustrine deposit examined by the Mars Science Laboratory mission. Experimental results showed that the deposition of fine-grained basaltic sediment leads to pore water chemistries that may trigger the precipitation of  $\text{Fe}(\text{OH})_2$  if pH increased to values of  $\sim 8.0$  and above. Interestingly,  $\text{Fe}(\text{OH})_2$ , once precipitated from water, is highly unstable in anoxic solutions at these pH levels; the authors documented that  $\text{Fe}(\text{OH})_2$  decomposes to green rust in a matter of minutes.  $\text{Fe}(\text{OH})_2$  is, in fact, a sufficiently strong electron donor that it reduces  $\text{H}_2\text{O}(\text{l})$ , generating  $\text{H}_2(\text{aq})$  in the process. Some of the structural Fe within  $\text{Fe}(\text{OH})_2$  itself oxidises during this process, generating octahedral layers composed of Fe(II) and Fe(III); the intercalation of anions from solution into interlayers satisfies the resulting charge imbalance and results in green rust formation. Given the structural similarity between  $\text{Fe}(\text{OH})_2$  and green rust, this mechanism offers a straight-forward pathway to form Fe(II)-Fe(III)-bearing double layer hydroxides under strictly anoxic conditions. Because, under the conditions investigated, green rust is metastable with respect to magnetite, the latter mineral was generated via dissolution/reprecipitation in a matter of days [82]. Although this pathway may be applicable to magnetite observed in Precambrian iron formation, petrographic constraints on the relative timing of magnetite precipitation will be critical. Because experimental data suggest that the rates of  $\text{Fe}(\text{OH})_2$  decomposition appear to be rapid, the sedimentological expression of this pathway are likely to generate syndepositional or very early diagenetic magnetite rather than fabric destructive magnetite (i.e., more likely a product of siderite decomposition).

These two studies offer additional intriguing pathways for the formation of minerals observed in iron formation and other Precambrian sediments through reactive intermediates. One pathway depends on



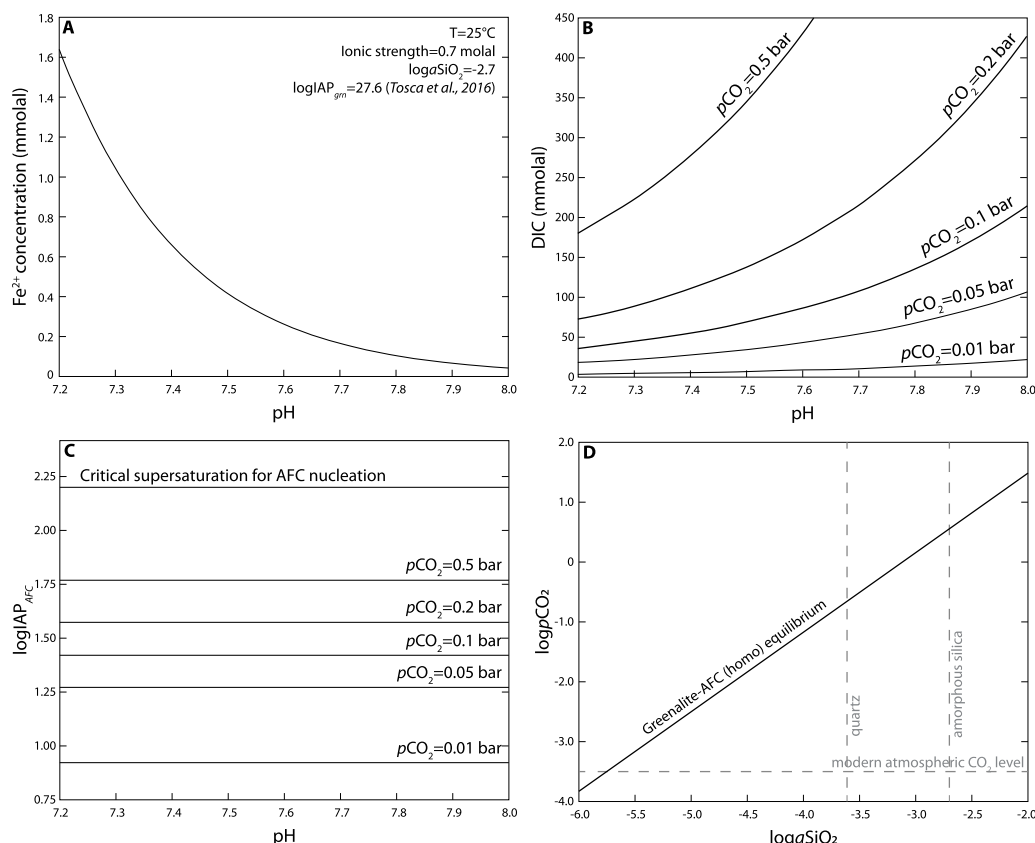


**Fig. 8.** Maximum  $\text{Fe}^{2+}$  concentration limited by greenalite apparent solubility (Tosca et al., 2016) for conditions relevant to Archean seawater. (B). Total dissolved inorganic carbon (DIC) at equilibria with various levels of  $p\text{CO}_2$  in Precambrian seawater. (C). AFC saturation state under various levels of  $p\text{CO}_2$  with  $\text{Fe}^{2+}$  concentration controlled by greenalite apparent solubility. Critical supersaturation for AFC nucleation is plotted as black solid line. (D). Requisite  $p\text{CO}_2$  level for homogeneous AFC precipitation at equilibrium with greenalite as a function of silica concentration. Dashed lines indicate quartz [118] and amorphous silica solubility.

oxic conditions, and the other operates under anoxic conditions. Although these studies may inform our understanding of the early Fe cycle, anion concentration is key to the formation and stability of green rust, in both oxic and anoxic pathways [83]. For example, because Halevy et al. (2017) conducted green rust syntheses at maximum  $\text{SiO}_2(\text{aq})$  concentrations of 0.25 mmol/kg (compared to amorphous silica saturation at  $\sim 2.2$  mmol/kg), it is unclear whether elevated  $\text{SiO}_2(\text{aq})$  concentrations might influence the kinetics of green rust precipitation and/or the ageing process. Similarly, experimental results obtained for the anoxic pathway [82] involved only slightly higher concentrations of  $\text{SiO}_2(\text{aq})$  ( $\sim 0.5$  mmol/kg), but still relatively low compared to amorphous silica saturation. In addition, high-resolution petrographic constraints on mineral paragenesis will continue to prove crucial in evaluating whether these mechanisms operated, and if so, whether they were important pathways that could have influenced the ancient iron cycle.

#### 4. The Archean iron cycle: merging sedimentological and geochemical constraints

New results from high-resolution petrography and experimental geochemistry place a number of constraints on the nature of the ancient Fe cycle and the major mineral sinks that balanced the supply of soluble  $\text{Fe}^{2+}$  to Archean marine basins. Recent petrographic studies indicate that: (1) abundant Fe(II)-silicates were delivered to deep water environments and formed the principal building blocks of iron formation, and (2) Fe(II)-carbonate was a common and important diagenetic product. At the same time, recent experimental geochemical studies

indicate that: (3) Fe(II)-silicate precipitation likely acted as a key reaction limiting the concentrations of dissolved  $\text{Fe}^{2+}$  in Archean seawater, and (4) the spontaneous precipitation of Fe(II)-carbonate from seawater (i.e., homogeneous nucleation) was unlikely to be an important process controlling  $\text{Fe}^{2+}$  concentrations in Archean seawater. Although green rust phases may have represented yet another important sink for Fe, their potential importance to iron formation is unclear. This is mainly because observational data collected on Archean iron formation cannot uniquely identify green rust transformation products, and iron formation mineralogy and paragenesis appears, at present, consistent with dominantly anoxic processes. Here we discuss an emerging view of the Archean iron cycle that is consistent with these four conclusions. Central to this view, however, and in reconciling the four conclusions listed above, is understanding what process(es) supplied voluminous Fe(II)-silicate sediment to Archean basinal environments, and assessing the impact of early diagenetic (i.e., heterogeneous) Fe(II)-carbonate precipitation as a potentially significant sink for  $\text{Fe}^{2+}$ .

##### 4.1. Hydrothermal effluent-seawater mixing and the origin of Fe(II)-silicates in iron formation

As discussed above, new high resolution microscopic data indicate that Archean and early Palaeoproterozoic iron formation were associated with the widespread production of Fe(II)-silicates (mainly greenalite) [11,21,28,55,66,67]. Accordingly, the extent to which these deposits inform our view of the early Fe cycle rests on understanding the origin of their major building blocks, the Fe(II)-silicates. Although

recent experimental work provides insight into spontaneous nucleation of Fe(II)-silicates from seawater at 25 °C, it is unclear whether low temperature precipitation from the ambient water column is capable of accounting for the emplacement of extensive Fe(II)-silicate-rich chemical muds. This conclusion is supported by stratigraphic and sedimentological relationships of iron formation intervals within the Hamersley Group, which are most consistent with deposition via density currents and subsequent re-working of chemical muds along the seafloor by bottom water currents or gravity-driven turbidity currents [84,85]. These observations suggest that the original sediments were deposited on the flanks of submarine volcanoes and the accumulation of iron formation precursor sediment was linked to periods of high relative sea level and/or vigorous hydrothermal activity, perhaps driven by pulses of seafloor spreading [84,85]. Because the major iron formation deposits of the Hamersley Group are inconsistent with pelagites derived by particle settling out of the water column [84,85], another process must have generated and re-deposited Fe(II)-silicates specifically in deep water basinal environments.

Much of the uncertainty relating to the origins of voluminous Fe(II)-silicate production in basinal settings relates to how exactly ambient seawater was modified by hydrothermal input. Rasmussen et al. (2017), in their analysis of iron formation deposits of the Transvaal Supergroup, suggested that hydrothermal effluent and ambient seawater chemically interacted to produce a plume of Fe(II)-silicate particles ultimately deposited at the seafloor. They envisioned that precipitation was triggered upon mixing acidic hydrothermal fluids rich in  $\text{Fe}^{2+}$  and  $\text{SiO}_2(\text{aq})$  with relatively alkaline ambient seawater to generate greenalite. This hypothesis can, in fact, be examined and tested in light of available constraints on Precambrian hydrothermal effluent chemistry and ambient seawater.

In their consideration of the effluent chemistry of Precambrian hydrothermal systems, Kump & Seyfried (2005) [86] noted that the interaction between low- $\text{SO}_4$  seawater and basalt in on-axis hydrothermal reaction zones would have driven the production of hydrothermal effluent enriched in  $\text{Fe}^{2+}(\text{aq})$ . This is because  $\text{SO}_4$  is a major oxidant that helps buffer the Fe–S–O subsystem in reaction zones at mid-ocean ridges today, and so low concentrations of  $\text{SO}_4$  in Precambrian seawater would have buffered the fluid interacting with basalt at a more reduced chemical state [87,88]. This influence, in combination with the strong complexation of  $\text{Fe}^{2+}$  by Cl species at elevated temperatures and pressures [89], would have generated hydrothermal effluent fluids associated with high  $\text{Fe}^{2+}/\text{H}_2\text{S}$  ratios. This effect would be particularly magnified at relatively low reaction zone pressures (i.e., 400 bar and lower, owing to P–T effects on Fe complexation [89]). Such low pressures are thought to have been more common in mid-ocean ridge systems developed during the Archean when higher heat flow led to shallower depths to the magma chamber [86,89,90].

Although they examined mixing and cooling of modelled hydrothermal effluent in the presence of oxygenated seawater, Kump & Seyfried (2005) did not examine mixing with anoxic seawater, which is of particular interest given recent constraints on iron formation precursor mineralogy. In modern black smoker systems, mineral precipitation is triggered upon mixing between hot effluent fluids (on the order of 250 °C upon expulsion at the seafloor [88]) with cold ambient seawater, both within and near the vent itself [91]. Because modern hydrothermal effluent is characterised by high  $\text{H}_2\text{S}/\text{Fe}$  ratios, most Fe is titrated out as pyrite, which is only a minor component of many black smoker mineral assemblages today [91–93]. But what precipitates might have characterised mid-ocean ridge systems in the Precambrian when seawater was anoxic and hydrothermal effluent characterised by a high  $\text{Fe}/\text{H}_2\text{S}$  ratio?

To examine this process, we can investigate the simple mixing between generalised hydrothermal effluent (following Kump & Seyfried (2005)) and Precambrian seawater (i.e., anoxic and  $\text{SiO}_2(\text{aq})$  concentrations at or near amorphous silica solubility) (Fig. 9). These simple calculations show that, depending on the amount of magmatic  $\text{H}_2\text{S}(\text{aq})$

delivered to seafloor vents (ultimately derived from pyrrhotite equilibria in the subsurface reaction zone [86]), mineral assemblages are likely to be dominated by greenalite and siderite with minor pyrite (Fig. 9). Although this calculation greatly simplifies a rather complicated physical process, similar approaches have successfully explained the origin of mineral species produced at modern black smokers [91].

The amounts of greenalite and siderite precipitated at Precambrian hydrothermal vents are, of course, dependent on the Fe and  $\text{SiO}_2(\text{aq})$  concentrations of the effluent fluid. These concentrations could have been modified during cooling and decompression as the reaction fluid was separated from the rock buffer and ascended through the oceanic crust [88,94]. Interestingly, these calculations show that much of the  $\text{SiO}_2(\text{aq})$  delivered to seafloor vent systems is determined by quartz solubility at elevated temperature and pressure, rather than ambient  $\text{SiO}_2(\text{aq})$  in seawater [95]. Iron, on the other hand, may be influenced by Fe-chlorite precipitation during cooling and decompression as fluids ascend through the oceanic crust. Fe-chlorite is a common product of sub-seafloor alteration assemblages; this may have attenuated  $\text{Fe}^{2+}$  in reaction fluids, in turn modifying minerals precipitated upon venting at the seafloor [88,94,96]. Nevertheless, if even broadly correct, such a hypothesis would provide one way to reconcile the stratigraphy, sedimentology, and geochemistry of major Archean iron formation deposits. In addition, a hydrothermal origin for at least some siderite produced at hydrothermal vent systems offers an additional interpretation for the systematically depleted  $\delta^{13}\text{C}$  values associated with some banded micritic siderite, originally thought to reflect primary sedimentation, as observed in iron formation of the Transvaal Supergroup [97]. Given that recent data suggest that fluxes of oxidised Fe to iron formation precursor sediments appears to have been limited, the  $\delta^{13}\text{C}$  composition of iron formation carbonates may in fact be consistent with simple mixing between a mantle  $\text{CO}_2$  source (assuming its isotopic composition, currently  $\delta^{13}\text{C}$  of approximately  $-6$ , has not changed through time) and ambient seawater [17]. Because the precipitation of hydrothermally derived iron may also, under some circumstances, give rise to depleted Fe isotope compositions [98,99], this offers an additional interpretation for some instances where iron formation carbonates retain isotopic compositions depleted in both  $\delta^{56}\text{Fe}$  and  $\delta^{13}\text{C}$  [65].

Finally, mixing calculations (Fig. 9) show that mineral precipitation upon fluid venting would have significantly decreased  $\text{Fe}^{2+}$  concentrations relative to current estimates; our calculations commonly estimate dissolved  $\text{Fe}^{2+}$  concentrations on the order of 1–3 mmol/kg following mineral precipitation upon venting and mixing with seawater. In fact, these concentrations can be considered upper estimates given that  $\text{Fe}^{2+}$  may be further attenuated as Fe-chlorite precipitates upon the ascension of hydrothermal fluids through the oceanic crust [88] and through mineral precipitation triggered by conductive heating and subsequent mixing of seawater within vent structures prior to venting at the seafloor [91].

If mineral precipitation would have strongly attenuated  $\text{Fe}^{2+}$  fluxes to Archean hydrothermal fluids, then how could this process have impacted globally averaged  $\text{Fe}^{2+}$  fluxes to Archean oceans? One approach to estimating the impact on  $\text{Fe}^{2+}$  fluxes is to estimate average post-precipitation  $\text{Fe}^{2+}$  concentrations of hydrothermal fluids and multiply this value by the amount of water thought to circulate through axial ridge systems. If precipitation commonly left 1–3 mmol/kg  $\text{Fe}^{2+}$  released to seawater after fluid mixing, then using modern estimates of water fluxes out of near axis hydrothermal vents ( $3 \times 10^{13}$  l/year [100]) leads to globally averaged hydrothermal fluxes of  $\sim 0.1\text{--}0.2 \times 10^{12}$  mol  $\text{Fe}^{2+}$ /year, strikingly similar to modern values [100]. Hydrothermal water fluxes, however, may have been higher than present for the Archean [101], but some have argued that they may have been lower [102]. In addition, shallower ridge systems might have favoured higher Fe concentrations through low pressure Fe–Cl complexation effects and two-phase separation [86,89]. Despite this uncertainty, even if hydrothermal fluids contained much higher  $\text{Fe}^{2+}$  concentrations, mineral precipitation upon fluid venting would have

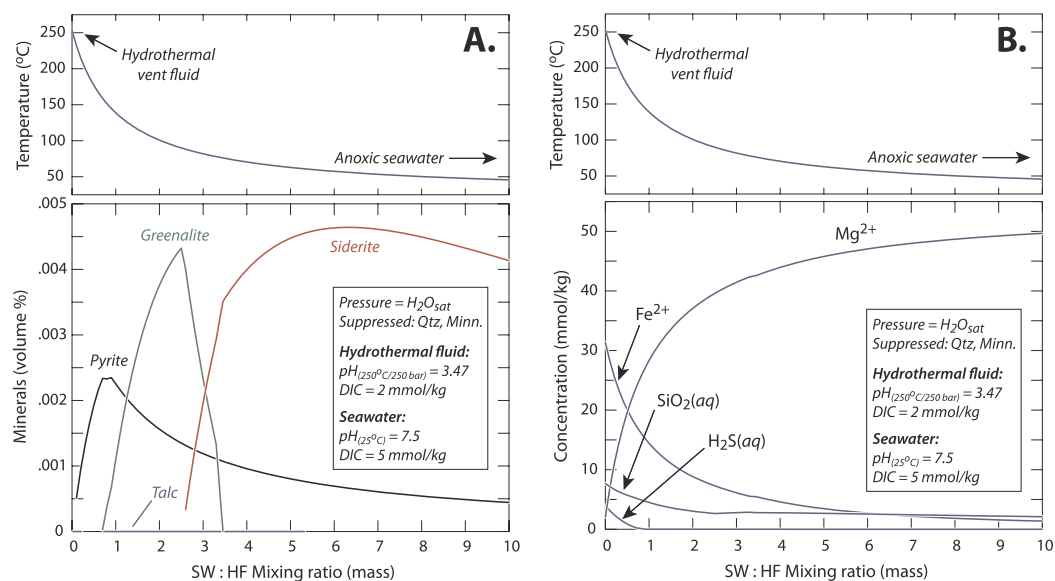


**Fig. 9.** Reaction path modelling of the mixing between hydrothermal effluent and anoxic seawater. Hydrothermal effluent composition is modelled after Kump & Seyfried (2005) ( $pH = 5$  at  $400^\circ C/400\text{ bar}$ ; Fe–S–O subsystem buffered by pyrrhotite-fayalite-magnetite-quartz equilibrium), and subsequently cooled and decompressed to  $250^\circ C/250\text{ bar}$  (allowing for pyrite and chlorite precipitation with decreasing temperature and pressure; Seyfried et al., 1997) to more closely represent conditions upon seafloor venting [88,119]. Seawater is based on modern composition but anoxic,  $SO_4$ -free, with a dissolved inorganic carbon (DIC) pool of 5 mmol/kg, and  $pH$  7.5. (A.) Minerals precipitated from fluid (back reaction is permitted) as a function of temperature and mixing ratio (by mass). Mineral assemblages are dominated by greenalite, siderite and lesser amounts of pyrite; these precipitate at low mixing ratios and elevated temperatures, indicating precipitation is likely to occur relatively close to seafloor vents. (B.) Evolution of fluid chemistry upon mixing between hydrothermal effluent and seawater.  $Fe^{2+}$  is rapidly depleted as minerals precipitate. Because  $Fe \gg H_2S(aq)$  (i.e., Kump & Seyfried, 2005),  $H_2S(aq)$  is quantitatively removed upon pyrite precipitation. Thermodynamic data were generated using SUPCRT92 via DBCreate ([120,121]), except for quartz solubility from Ref. [95] and Fe–Cl complexation constants from Ref. [89]. Quartz and minnesotaite were suppressed from forming because, although quartz controls  $SiO_2(aq)$  concentrations at reaction zone conditions, amorphous silica is likely to dominate silica polymorphs upon venting at the seafloor [119] and minnesotaite is widely recognised as a metamorphic product of greenalite [122,123].

remained a key process attenuating  $Fe^{2+}$  fluxes to the Archean ocean. This is because increases in  $Fe^{2+}$  concentrations, in most cases, simply lead to larger quantities of minerals precipitated upon venting and mixing.

Combining this estimate of hydrothermal  $Fe^{2+}$  fluxes with globally averaged riverine  $Fe^{2+}$  fluxes in turn allows us to estimate the total supply of  $Fe^{2+}$  to Archean oceans. Applying a generous estimate of averaged riverine  $Fe^{2+}$  fluxes (assuming ~65% of the continental crust was formed by 2.4 Ga [44], modern riverine water fluxes of  $4 \times 10^{16}\text{ L/yr}$  [100], and an average river water  $Fe^{2+}$  concentration of 0.112 mmol/L  $Fe^{2+}$ ; from Hao et al., 2017), yields total  $Fe^{2+}$  fluxes to the oceans that fall in the range of  $\sim 3 \times 10^{12}\text{ mol } Fe^{2+}/\text{year}$ . What processes might have balanced these  $Fe^{2+}$  sources and what are the implications for electron donor supply?

#### 4.2. Early diagenetic Fe(II)-carbonate precipitation as a deep water sink for $Fe^{2+}$

A variety of evidence supports the notion that early diagenetic siderite precipitation may have acted as a significant sink for hydrothermal  $Fe^{2+}$ , which would have further attenuated the soluble  $Fe^{2+}$  flux to the surface ocean. In addition to evidence for early diagenetic siderite precipitation in Hamersley Group iron formation [68], siderite is also an important early diagenetic constituent in clastic intervals of the Hamersley Group [70,85]. For example, Krapez et al. (2003) and Pickard et al. (2004) show that siderite is the earliest-forming and most common Fe-rich phase in clastic rocks throughout the Brockman Supersquence, sometimes forming siderite-rich partings punctuating detrital dolomitic sediments re-worked into continental shelf environments. In fact, similar lithofacies descriptions have been reported for iron formation deposited in the Krivoryog basin of the Ukraine [103]

and for iron formation intervals of the Kaapvaal Craton [97,104,105]. For example, Klein & Beukes (1989), Beukes & Klein (1990) and Kaufman et al. (1990) cite petrographic evidence for “primary” siderite, occurring as finely disseminated crystals comprising siderite-rich micro and mesobands. These studies refer to siderite as “microspar” which leaves open the possibility that siderite-rich sediments were deposited and then re-crystallised during early diagenesis or were formed *de novo* as a pore-filling cement during early diagenetic reactions in pore waters.

Fe isotope studies also indicate that the isotopic signature of siderite-rich siliciclastic sedimentary rocks is consistent with a hydrothermal source for Fe. For example, Yamaguchi et al. (2005) [65] noted that the average  $\delta^{56}Fe$  value of  $-0.5\%$  for siderite-enriched shales ranging from 3.3 to 2.2 Ga in age is best interpreted as a hydrothermal signature. Indeed, although typically assumed to be characterised by a  $\delta^{56}Fe$  value of close to zero in a dominantly anoxic ocean [64,65], studies of modern hydrothermal systems have shown significant variability in the  $\delta^{56}Fe$  values of fluids and sulphides from modern systems [99], as well as for altered segments of Mesozoic oceanic crust [98]. The processes responsible for isotopic variation in Precambrian systems and their range in composition is nevertheless deserving of continued study.

Early diagenetic siderite precipitation clearly represented an important process in distal slope to basinal settings [65,70,85,106] and, in the case of the Kuruman and Griquatown iron formations, across the full spectrum of depositional environments shortly after the drowning of the Campbellrand platform [107]. What conditions would have promoted early diagenetic siderite precipitation if nucleation of Fe(II)-carbonate from the water column was kinetically inhibited?

The experimental results of Jiang & Tosca (2019) [17] indicate that the spontaneous (homogeneous) precipitation of siderite from Archean



seawater was probably not a common process given that the supersaturation threshold was unlikely to have been reached in the Archean water column. However, Jiang & Tosca (2019) [17] suggested one likely possibility pertaining to the origin of Fe(II)-carbonate: that early diagenetic siderite precipitation was driven by the *heterogeneous* precipitation of Fe(II)-carbonate on pre-existing mineral surfaces. It is well understood from kinetic theory that certain particulate surfaces may catalyse the nucleation of a mineral if the solution is adequately supersaturated and the substrate possesses favourable characteristics [73,74,108,109]. Importantly, that a certain type of surface can initiate nucleation means that the threshold for supersaturation will be lower than the threshold for homogeneous nucleation (that is, the threshold identified by Jiang & Tosca, 2019). In order for a substrate to be suitable, however, the energetics of the interface between the precipitating cluster and the substrate ( $\sigma_{CS}$ ) must be more favourable than the interface between the precipitating cluster and the aqueous solution ( $\sigma_{CW}$ ) [73,74,108,109]. Such a surface should minimise the work involved in creating a precipitate cluster on a substrate and must have a solid-solution interfacial energy similar to that of the precipitate ( $\sigma_{SW} \approx \sigma_{CW}$ ). In addition, the surface must strongly adsorb the ions of the precipitate ( $\text{Fe}^{2+}$  and/or  $\text{CO}_3^{2-}$  in the case of siderite) and it must be present in sufficient amounts such that surface area is large (in other words, a few grains will not be sufficient to trigger significant heterogeneous nucleation) [73,74,108,109].

That early diagenetic siderite is commonly associated with greenalite-rich muds in iron formation intervals deposited on the Pilbara and Kaapvaal cratons (i.e., Rasmussen & Muhling, 2018; Beukes, 1984) suggests that greenalite may have satisfied the above criteria and acted as a favourable surface to trigger Fe(II)-carbonate nucleation. Although not yet understood quantitatively, it is likely that greenalite would adsorb  $\text{Fe}^{2+}$ , possess a high specific surface area, and, may also possess similar interfacial energy to initially-formed Fe(II)-carbonate nuclei (if AFC acted as a precursor phase) [73,108,110]. This logic may apply to amorphous silica as well, which is expected to possess similar energetic properties on the basis of surface energy-solubility correlations [110]. Finally, it is worth noting that both homogeneous and heterogeneous nucleation will occur simultaneously but that low degrees of supersaturation will always permit rates of heterogeneous nucleation to

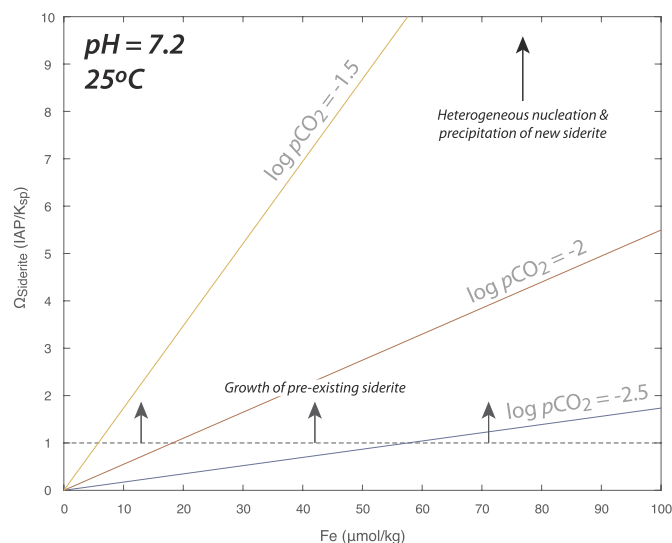


**Fig. 11.** Relationship between siderite supersaturation and Fe concentration as a function of  $p\text{CO}_2$  levels estimated for the late Archean [41]. Although the threshold for heterogeneous nucleation (i.e., Figure 15A) is unconstrained, it is likely to lie in a range lower than estimated for the homogeneous case by Jiang & Tosca (2019). Thus, at  $p\text{CO}_2$  levels relevant to the late Archean, transient  $\text{Fe}^{2+}$  concentrations less than 1 mmol/kg are likely to have triggered heterogeneous nucleation and the development of new Fe(II)-carbonate in sediments. However, growth of pre-existing siderite will occur at any omega value greater than 1.

dominate over homogeneous nucleation (Fig. 10) [73,108].

These constraints suggest that the heterogeneous precipitation of siderite on greenalite surfaces should be favoured at supersaturation levels less than the threshold identified by Jiang & Tosca (2019), but greater than siderite equilibrium. Although this threshold has not yet been determined, simple calculations show that, in light of current estimates of pH and  $p\text{CO}_2$  for the Archean ocean-atmosphere system [41,75,76], seawater may have commonly exceeded the threshold required for heterogeneous Fe(II)-carbonate nucleation. It is important to

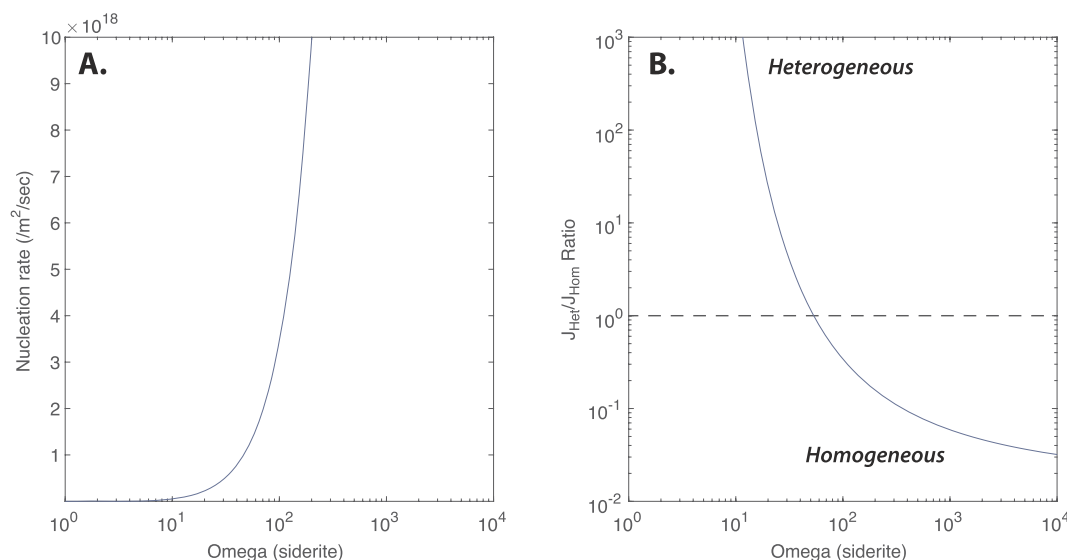


**Fig. 10.** (A.) Heterogeneous nucleation rate of siderite as a function of supersaturation ( $\Omega = \text{IAP}/K_{sp}$ ). Similar to homogeneous nucleation, kinetic theory predicts a strong exponential relationship between heterogeneous nucleation rates and supersaturation such that an effective threshold can be identified. Above this threshold, heterogeneous nucleation will dominate, and below this threshold, only crystal growth on pre-existing siderite crystals will occur (B.) The ratio of heterogeneous nucleation rate to the homogeneous nucleation rate of siderite as a function of supersaturation. At high supersaturation, homogeneous nucleation dominates. Calculations follow [124] where:  $\sigma = 50 \text{ mJ/m}^2$ , molar volume of siderite ( $v_m$ ) =  $2.938 \times 10^{-5} \text{ m}^3/\text{mol}$ ,  $K_{ad}$ , or the linear sorption coefficient = 1000,  $K_{ad}^0 = 100$ , saturation concentration is based on Jiang & Tosca (2019), and  $\Delta G_{in} = 50 \text{ kJ/mol}$ .

note that this may only require relatively low bottom water Fe concentrations, which are in turn dependent on ambient pH (Fig. 11). Another possibility is that Fe concentrations in sediment pore waters may have been buffered by Fe(II)-silicate dissolution. This result leaves open the possibility early diagenetic siderite may have precipitated inorganically without the assistance of Fe-reducing bacteria, if the Fe concentration in pore waters was influenced by greenalite solubility.

Regardless of whether siderite initially existed in iron formation precursor sediments through deposition as a hydrothermal precipitate or through initial heterogeneous nucleation, diagenetic siderite crystal growth (as opposed to nucleation) would have acted as a sink for  $\text{Fe}^{2+}$  whenever Fe-rich sediments maintained diffusional contact with the overlying water column. As discussed above, petrographic evidence for early diagenetic siderite in chemical and clastic deep water sediments of the Brockman Supersequence suggest that this process continued as sediments were re-worked along the basin floor. How significant of a sink for  $\text{Fe}^{2+}$  would diagenetic siderite growth have been to the Archean Fe cycle?

As an instructive calculation, we can consider the global impact of diagenetic siderite precipitation in the Hamersley Group alone. First we assume that deep water chemical and clastic sediments occupied an area equivalent to the current estimated area of the Hamersley Group ( $\sim 80,000 \text{ km}^2$ ), that the upper 50 cm of sediment was active during early diagenesis, and that the sediments were characterised by 75% porosity (pre-compaction), and contained initially 1% siderite by volume. The most significant source of uncertainty in this calculation relates to the siderite growth rate at low saturation. Reported rate constants for surface area normalised siderite growth vary considerably [111–113]. Nevertheless, using minimum measured laboratory rates for siderite growth ( $\sim 1.69 \mu\text{mol}/\text{m}^2/\text{hr}$  [112]) and assuming a representative specific surface area for siderite ( $\sim 1 \text{ m}^2/\text{g}$  [112]) leads to an estimated flux of  $5.8 \times 10^{12} \text{ mol}/\text{year}$   $\text{Fe}^{2+}$  from Hamersley Group sediments alone. This flux is of the same order as our combined estimate of globally averaged riverine and hydrothermal  $\text{Fe}^{2+}$  fluxes to the oceans discussed above (Fig. 12). These estimates may underestimate the potential impact of diagenetic siderite precipitation on the  $\text{Fe}^{2+}$  cycle. For example, if siderite saturation in sedimentary pore waters was higher, crystal growth rates could increase to one or even two orders of magnitude beyond those used here, depending on the nature of the precipitation rate law [112].

Together, observational constraints on Precambrian Fe-rich rocks, kinetic theory, and limited experimental data suggest that the early diagenetic growth of siderite on pre-existing chemical sediments (especially greenalite and/or amorphous silica) likely represented an important sink for  $\text{Fe}^{2+}$ . This process appears to have continued somewhat independently of iron formation deposition itself (i.e. [70,85]), and occasionally operated across a spectrum of depositional environments [107]. Conservative estimates suggest that this diagenetic sink may have quantitatively balanced  $\text{Fe}^{2+}$  fluxes into the Archean

oceans. Thus, the late Archean iron cycle was strongly governed by the kinetics of Fe(II)-mineral precipitation (and dissolution) processes that internally recycled Fe delivered in both particulate and soluble forms from riverine and hydrothermal sources. Depending on reaction kinetics and oceanographic transport processes, diagenetic growth of pre-existing (i.e., hydrothermally-derived) or new Fe(II)-carbonate in sedimentary pore waters may have significantly attenuated late Archean steady state marine  $\text{Fe}^{2+}$  concentrations. Our analysis also implies that future experimental work on the precipitation kinetics of Fe(II)-carbonate should provide quantitative tools to more completely model the Fe cycle and also place constraints on ocean carbonate chemistry associated with early diagenesis of deep (and some shallow) water sediments.

## 5. Implications and future directions

Recent advances in high resolution petrography of Fe-rich chemical sediments has refined our view of the dominant mineral products of the Fe cycle on the early Earth. At the same time, new constraints from experimental and theoretical geochemistry have led to a more nuanced understanding of the rates and mechanisms behind Fe-based chemical sedimentation on the early Earth. Although much more work remains, these new constraints together suggest that the supply of  $\text{Fe}^{2+}$  to Archean oceans was controlled by the interplay between hydrothermal-seawater mixing (and the subsequent transport and reactivity of chemical sediments along the seafloor), early diagenetic Fe(II)-carbonate precipitation, and, potentially, authigenic greenalite precipitation from the water column or sediment pore waters (Fig. 12). Most importantly, and in contrast with existing models, recent petrographic analyses and geochemical modelling indicate much of the Fe currently hosted in Precambrian iron formation and siliciclastic sediments was delivered to marine basins dominantly in particulate form rather than in dissolved form. From a mass balance point of view, this conclusion is consistent with those reached by Kump & Holland (1992) [45] and clarifies the mechanisms and mineral products of the Fe enrichment long recognized as a distinctive feature of Precambrian rocks. Simple estimates of the impact of hydrothermal-seawater mixing and diagenetic Fe(II)-carbonate precipitation indicate that  $\text{Fe}^{2+}$  supplied to the oceans may have been quantitatively balanced by chemical and clastic sediment diagenesis.

The view of the Fe cycle presented here makes predictions for the sedimentary and mineralogical expression of exceeding critical thresholds in dissolved  $\text{Fe}^{2+}$  concentrations. For example, although experimental work helps identify the chemical processes associated with spontaneous nucleation of Fe-bearing mineral phases from the water column, unique geological evidence for Fe-bearing precipitates that were formed in the water column remains limited. Indeed, given the likelihood that diagenetic Fe(II)-carbonate production balanced soluble  $\text{Fe}^{2+}$ , it remains possible that Archean marine  $\text{Fe}^{2+}$

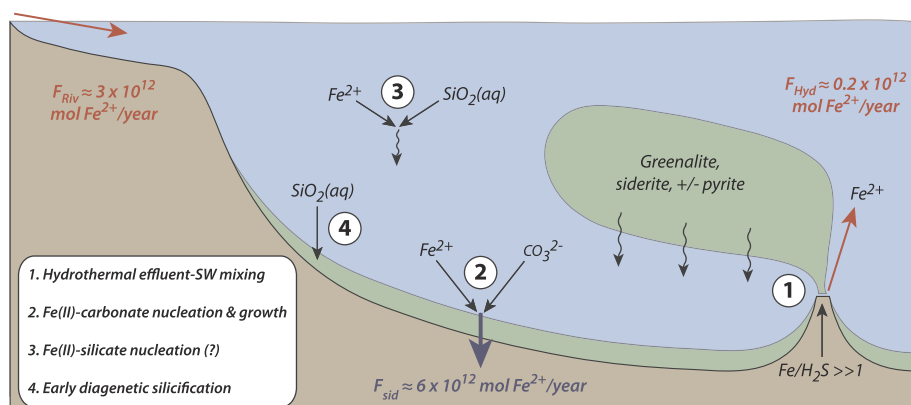


**Fig. 12.** Schematic of the Fe cycle before the oxygenation of the oceans and atmosphere (i.e., before the GOE). Because of mineral precipitation upon mixing, soluble hydrothermal  $\text{Fe}^{2+}$  fluxes into the oceans are likely to lie within the range of modern hydrothermal  $\text{Fe}^{2+}$  fluxes, based in simple mixing calculations (i.e., Figure 14). If, as the rock record suggests, clastic and/or chemical deep water sediments initially contained 1 vol percent siderite (either through hydrothermal particulate input or through transient heterogeneous nucleation), near equilibrium siderite growth rates within the upper 50 cm of the sediment across an area equivalent to the Hamersley Basin could have balanced or even exceeded global Fe inputs into the ocean (i.e.,  $F_{\text{sid}} = \sim 6 \times 10^{12} \text{ mol Fe}^{2+}/\text{year}$ ).

concentrations may have only rarely reached levels where spontaneous precipitation of greenalite could have occurred in the water column. Continued interrogation of the ancient rock record, and detailed quantification of the fluxes associated with early diagenetic siderite precipitation will help provide a more definitive answer.

Finally, the view of the early Fe cycle presented here carries significant implications for our current understanding of electron donor availability before the advent of oxygenic photosynthesis. For example, even if early diagenetic siderite precipitation is neglected as a potentially important sink for  $\text{Fe}^{2+}$ , total  $\text{Fe}^{2+}$  fluxes delivered to Archean oceans would only have global primary productivity at a level over  $5000\times$  less than today (if other nutrients were non-limiting [114]). This is consistent with recent suggestions (Ward et al., 2019) [4] that primary productivity before oxygenic photosynthesis may have been severely limited by electron donors rather than N or P (Ward et al., 2019) [4]. Although an in depth understanding of hydrothermal vent fluid chemistry, mixing, and the chemical dynamics of Fe(II)-carbonate diagenesis is required to refine these estimates, this overall conclusion is not likely to change; available constraints suggests that Fe played a negligible role, at best, in supporting primary productivity on the early Earth.

## Acknowledgements

The authors thank Woody Fischer and Joan Valentine for the invitation to contribute to this volume, as well as Lee Kump and an anonymous reviewer for comments that improved the clarity of this manuscript. NJT acknowledges NERC grant NE/M013014/1 and Leverhulme Trust grant PLP-2015-286.

## Appendix A. Supplementary data

Supplementary data to this article can be found online at <https://doi.org/10.1016/j.freeradbiomed.2019.05.005>.

## References

- [1] R.M. Garrels, E. Perry, Cycling of carbon, sulfur, and oxygen through geologic time, *Sea* 5 (1974) 303–336.
- [2] D.E. Canfield, M.T. Rosing, C. Bjerrum, Early anaerobic metabolisms, *Phil. Trans. Biol. Sci.* 361 (2006) 1819.
- [3] P. Kharecha, J. Kasting, J. Siefert, A coupled atmosphere–ecosystem model of the early Archean Earth, *Geobiology* 3 (2005) 53–76.
- [4] L. Ward, B. Rasmussen, W. Fischer, Primary productivity was limited by electron donors prior to the advent of oxygenic photosynthesis, *J. Geophys. Res.: Biogeosciences* 124 (2) (2019) 211–226.
- [5] H.D. Holland, The oceans; a possible source of iron in iron-formations, *Econ. Geol.* 68 (1973) 1169–1172.
- [6] H. Holland, *The Chemical Evolution of the Atmosphere and Oceans*, Princeton University Press, Princeton, NJ, 1984.
- [7] H.P. Eugster, I.-M. Chou, The depositional environments of Precambrian banded iron-formations, *Econ. Geol.* 68 (1973) 1144–1168.
- [8] J.L. Drever, Geochemical model for the origin of Precambrian banded iron formations, *Geol. Soc. Am. Bull.* 85 (1974) 1099.
- [9] J.E. Johnson, S.M. Webb, K. Thomas, S. Ono, J.L. Kirschvink, W.W. Fischer, Manganese-oxidizing photosynthesis before the rise of cyanobacteria, *Proc Natl Acad Sci U S A*, 2013.
- [10] W.W. Fischer, D.A. Fike, J.E. Johnson, T.D. Raub, Y. Guan, J.L. Kirschvink, J.M. Eiler, SQUID-SIMS is a useful approach to uncover primary signals in the Archean sulfur cycle, *Proc Natl Acad Sci U S A*, 2014.
- [11] B. Rasmussen, J.R. Muhling, A. Suvorova, B. Krapež, Greenalite precipitation linked to the deposition of banded iron formations downslope from a late Archean carbonate platform, *Precambrian Res.* 290 (2017) 49–62.
- [12] J.E. Johnson, J.R. Muhling, J. Cosmidis, B. Rasmussen, A.S. Templeton, Low-Fe (III) greenalite was a primary mineral from Neoproterozoic oceans, *Geophys. Res. Lett.* 45 (2018) 3182–3192.
- [13] G. Paris, J.F. Adkins, A.L. Sessions, S.M. Webb, W.W. Fischer, Neoproterozoic carbonate-associated sulfate records positive  $\Delta^{34}\text{S}$  anomalies, *Science* 346 (2014) 739–741.
- [14] I. Halevy, M. Alesker, E. Schuster, R. Popovitz-Biro, Y. Feldman, A key role for green rust in the Precambrian oceans and the genesis of iron formations, *Nat. Geosci.* 10 (2) (2017) 135–139.
- [15] N.J. Tosca, S. Guggenheim, P.K. Pufahl, An authigenic origin for Precambrian greenalite: implications for iron formation and the chemistry of ancient seawater, *Geol. Soc. Am. Bull.* 128 (2016) 511–530.
- [16] N.J. Tosca, I. Ahmed, B. Tutolo, A. Ashpittel, J. Hurowitz, Magnetite authigenesis and the warming of early Mars, *Nat. Geosci.* 11 (9) (2018) 635–639.
- [17] C.Z. Jiang, N.J. Tosca, Fe(II)-carbonate precipitation kinetics and the chemistry of anoxic ferruginous seawater, *Earth Planet. Sci. Lett.* 506 (2019) 231–242.
- [18] H.D. Holland, The geologic history of seawater, *Treatise Geochem.* 6 (2003) 583–625.
- [19] R. Siever, The silica cycle in the Precambrian, *Geochem. Cosmochim. Acta* 56 (1992) 3265–3272.
- [20] R.G. Maliva, A.H. Knoll, B.M. Simonson, Secular change in the Precambrian silica cycle: insights from chert petrology, *Geol. Soc. Am. Bull.* 117 (2005) 835–845.
- [21] B. Rasmussen, B. Krapež, J.R. Muhling, A. Suvorova, Precipitation of Iron Silicate Nanoparticles in Early Precambrian Oceans Marks Earth's First Iron Age, *Geology*, (2015).
- [22] E.J.T. Stefurak, R. Lowe, D. Zentner, W. Fischer, Primary silica granules—A new mode of Paleoproterozoic sedimentation, *Geology* 42 (2014) 283–286.
- [23] E.J. Stefurak, W.W. Fischer, D.R. Lowe, Texture-specific Si isotope variations in Barberton Greenstone Belt cherts record low temperature fractionations in early Archean seawater, *Geochem. Cosmochim. Acta* 150 (2015) 26–52.
- [24] E.J. Stefurak, D.R. Lowe, D. Zentner, W.W. Fischer, Sedimentology and geochemistry of Archean silica granules, *Geol. Soc. Am. Bull.* B31181 1 (2015).
- [25] P.J. Tréguer, C.L. De La Rocha, The world ocean silica cycle, *Ann Rev Mar Sci* 5 (2013) 477–501.
- [26] D.R. Lowe, Archean sedimentation, *Annu. Rev. Earth Planet Sci.* 8 (1980) 145–167.
- [27] D.R. Lowe, Restricted shallow-water sedimentation of early Archean stromatolitic and evaporitic strata of the strelley pool chert, Pilbara block, Western Australia, *Precambrian Res.* 19 (1983) 239–283.
- [28] B. Rasmussen, B. Krapež, J.R. Muhling, Seafloor Silicification and Hardground Development during Deposition of 2.5 Ga Banded Iron Formations, *Geology*, (2015).
- [29] R.G. Maliva, A.H. Knoll, R. Siever, Secular change in chert distribution: a reflection of evolving biological participation in the silica cycle, *Palaio* 4 (1989) 519–532.
- [30] W.W. Fischer, A.H. Knoll, An iron shuttle for deepwater silica in Late Archean and early Paleoproterozoic iron formation, *Geol. Soc. Am. Bull.* 121 (2009) 222–235.
- [31] L.A. Williams, D.A. Crerar, Silica diagenesis; II, General mechanisms, *J. Sediment. Res.* 55 (1985) 312.
- [32] R.K. Iler, *The Chemistry of Silica: Solubility, Polymerization, Colloid and Surface Properties, and Biochemistry*, Wiley, New York, 1979.
- [33] S.H.J.M. van den Boorn, M.J. van Bergen, W. Nijman, P.Z. Vroon, Dual role of seawater and hydrothermal fluids in Early Archean chert formation: evidence from silicon isotopes, *Geology* 35 (2007) 939–942.
- [34] R. Chakrabarti, A.H. Knoll, S.B. Jacobsen, W.W. Fischer, Si isotope variability in Proterozoic cherts, *Geochem. Cosmochim. Acta* 91 (2012) 187–201.
- [35] J.P. Grotzinger, N.P. James, Precambrian Carbonates: Evolution of Understanding, vol. 67, SEPM Special Publication, 2000, pp. 3–20.
- [36] D.Y. Sumner, J.P. Grotzinger, Implications for Neoproterozoic ocean chemistry from primary carbonate mineralogy of the Campbellrand-Malmani Platform, South Africa, *Sedimentology* 51 (2004) 1273–1299.
- [37] D.Y. Sumner, J.P. Grotzinger, Late Archean Aragonite Precipitation: Petrography, Facies Associations, and Environmental Significance vol. 67, SEPM Special Publication, 2000.
- [38] J.P. Grotzinger, Facies and evolution of Precambrian carbonate depositional systems: emergence of the modern platform archetype, *Controls Carbonates platform Basin Dev.* 44 (1989) 79–106.
- [39] J.P. Grotzinger, Geochemical model for Proterozoic stromatolite decline, *Am. J. Sci.* 290A (1990) 80–103.
- [40] J.A. Higgins, W.W. Fischer, D.P. Schrag, Oxygenation of the ocean and sediments: consequences for the seafloor carbonate factory, *Earth Planet. Sci. Lett.* 284 (2009) 25–33.
- [41] C.L. Blättler, L.R. Kump, W.W. Fischer, G. Paris, J.J. Kasbohm, J.A. Higgins, Constraints on ocean carbonate chemistry and  $\text{pCO}_2$  in the Archean and Palaeoproterozoic, *Nat. Geosci.* 10 (1) (2016) 41–45.
- [42] R.M. Garrels, F.T. Mackenzie, *Evolution of Sedimentary Rocks*, Norton, New York, 1971.
- [43] S.M. McLennan, On the geochemical evolution of sedimentary rocks, *Earth Sci. Rev.* 37 (1982) 335–350.
- [44] S.R. Taylor, S.M. McLennan, *The Continental Crust: its Composition and Evolution*, Blackwell, Oxford, 1985.
- [45] L.R. Kump, H.D. Holland, Iron in Precambrian rocks: implications for the global oxygen budget of the ancient Earth, *Geochem. Cosmochim. Acta* 56 (1992) 3217–3223.
- [46] A. Bekker, J.F. Slack, N. Planavsky, B. Krapež, A. Hofmann, K.O. Konhauser, O.J. Rouxel, Iron formation: the sedimentary product of a complex interplay among mantle, tectonic, oceanic, and biospheric processes, *Econ. Geol.* 105 (2010) 467.
- [47] H.L. James, Sedimentary facies of iron-formation, *Econ. Geol.* 49 (1954) 235–293.
- [48] E. Spencer, F.G. Percival, The structure and origin of the banded hematite jaspers of Singhbhum, India, *Econ. Geol.* 47 (1952) 365–383.
- [49] D.E. Ayres, Genesis of iron-bearing minerals in banded Iron Formation mesobands in the Dales Gorge member, Hamersley group, Western Australia, *Econ. Geol.* 67 (1972) 1214–1233.
- [50] E. Dimroth, J.-J. Chauvel, Petrography of the sokoman iron formation in part of the central Labrador trough, Quebec, Canada, *Geol. Soc. Am. Bull.* 84 (1973) 111.
- [51] N.J. Beukes, J. Gutzmer, Origin and paleoenvironmental significance of major iron



- formations at the Archean-Paleoproterozoic boundary, *Rev. Econ. Geol.* 15 (2008) 5–47.
- [52] S. Sun, K.O. Konhauser, A. Kappler, Y. Li, Primary Hematite in Neoproterozoic Oceans, *Geological Society of America Bulletin*, 2015.
  - [53] G.L. LaBerge, Development of magnetite in iron formations of the Lake Superior region, *Econ. Geol.* 59 (1964) 1313–1342.
  - [54] W.C. Krumbein, R.M. Garrels, Origin and classification of chemical sediments in terms of pH and oxidation-reduction potentials, *J. Geol.* 60 (1952) 1–33.
  - [55] B. Rasmussen, J.R. Muhling, A. Suvorova, B. Krapež, Dust to dust: evidence for the formation of “primary” hematite dust in banded iron formations via oxidation of iron silicate nanoparticles, *Precambrian Res.* 284 (2016) 49–63.
  - [56] P. Cloud, Paleocological significance of the banded iron-formation, *Econ. Geol.* 68 (1973) 1135–1143.
  - [57] P.S. Braterman, A.G. Cairns-Smith, R.W. Sloper, Photo-oxidation of hydrated  $\text{Fe}^{2+}$ -significance for banded iron formations, *Nature* 303 (1983) 163–164.
  - [58] K.O. Konhauser, L. Amskold, S.V. Lalonde, N.R. Posth, A. Kappler, A. Anbar, Decoupling photochemical Fe (II) oxidation from shallow-water BIF deposition, *Earth Planet. Sci. Lett.* 258 (2007) 87–100.
  - [59] K.O. Konhauser, N.J. Planavsky, D.S. Hardisty, L.J. Robbins, T.J. Warchola, R. Haugeard, S.V. Lalonde, C.A. Partin, P.B.H. Oonk, H. Tsikos, Iron Formations: A Global Record of Neoproterozoic to Paleoproterozoic Environmental History, *Earth-Science Reviews*, 2017.
  - [60] J.C.G. Walker, Suboxic diagenesis in banded iron formations, *Nature* 309 (1984) 340.
  - [61] K.O. Konhauser, D.K. Newman, A. Kappler, The potential significance of microbial Fe(III) reduction during deposition of Precambrian banded iron formations, *Geobiology* 3 (2005) 167–177.
  - [62] C.M. Johnson, J.M. Ludois, B.L. Beard, N.J. Beukes, A. Heimann, Iron formation carbonates: Paleocyanographic proxy or recorder of microbial diagenesis? *Geology* 41 (2013) 1147–1150.
  - [63] C.M. Johnson, E.E. Roden, S.A. Welch, B.L. Beard, Experimental constraints on Fe isotope fractionation during magnetite and Fe carbonate formation coupled to dissimilatory hydrous ferric oxide reduction, *Geochem. Cosmochim. Acta* 69 (2005) 963–993.
  - [64] C.M. Johnson, B.L. Beard, E.E. Roden, The iron isotope Fingerprints of redox and biogeochemical cycling in modern and ancient earth, *Annu. Rev. Earth Planet Sci.* 36 (2008) 457–493.
  - [65] K.E. Yamaguchi, C.M. Johnson, B.L. Beard, H. Ohmoto, Biogeochemical cycling of iron in the Archean-Paleoproterozoic Earth: constraints from iron isotope variations in sedimentary rocks from the Kaapvaal and Pilbara Cratons, *Chem. Geol.* 218 (2005) 135–169.
  - [66] B. Rasmussen, D.B. Meier, B. Krapež, J.R. Muhling, Iron silicate microgranules as precursor sediments to 2.5-billion-year-old banded iron formations, *Geology* 41 (2013) 435–438.
  - [67] B. Rasmussen, B. Krapež, D.B. Meier, Replacement origin for hematite in 2.5 Ga banded iron formation: evidence for postdepositional oxidation of iron-bearing minerals, *Geol. Soc. Am. Bull.* 126 (2014) 438–446.
  - [68] B. Rasmussen, J.R. Muhling, Making magnetite late again: evidence for widespread magnetite growth by thermal decomposition of siderite in Hamersley banded iron formations, *Precambrian Res.* 306 (2018) 64–93.
  - [69] V. Milesi, F. Guyot, F. Brunet, L. Richard, N. Recham, M. Benedetti, J. Dairou, A. Prinzhofer, The Formation of  $\text{CO}_2$ ,  $\text{H}_2$  and condensed carbon from siderite dissolution in the 200–300°C range and at 50MPa, *Geochem. Cosmochim. Acta* 154 (2015) 201–211.
  - [70] B. Krapež, M.E. Barley, A.L. Pickard, Hydrothermal and resedimented origins of the precursor sediments to banded iron formation: sedimentological evidence from the Early Palaeoproterozoic Brockman Supersequence of Western Australia, *Sedimentology* 50 (2003) 979–1011.
  - [71] K.S. Rybacki, L.R. Kump, E.J. Hanski, V.A. Melezhik, Weathering during the great oxidation event: Fennoscandia, arctic Russia 2.06 Ga ago, *Precambrian Res.* 275 (2016) 513–525.
  - [72] B. Rasmussen, B. Krapež, J.R. Muhling, Hematite Replacement of Iron-Bearing Precursor Sediments in the 3.46-b.y.-old Marble Bar Chert, Pilbara Craton, Australia, *Geological Society of America Bulletin*, 2014.
  - [73] P. van Cappellen, PhD. Thesis, The Formation of Marine Apatite: A Kinetic Study Yale University, (1991).
  - [74] A.C. Lasaga, H.D. Holland (Ed.), *Kinetic Theory in the Earth Sciences*, Princeton University Press, Princeton, NJ, 1998.
  - [75] I. Halevy, A. Bachan, The geologic history of seawater pH, *Science* 355 (2017) 1069–1071.
  - [76] J. Krissansen-Totton, G.N. Arney, D.C. Catling, Constraining the climate and ocean pH of the early Earth with a geological carbon cycle model, *Proc Natl Acad Sci U S A*, 2018.
  - [77] K. Dideriksen, C. Frandsen, N. Bovet, A.F. Wallace, O. Sel, T. Arbour, A. Navrotsky, J.J. De Yoreo, J.F. Banfield, Formation and transformation of a short range ordered iron carbonate precursor, *Geochem. Cosmochim. Acta* 164 (2015) 94–109.
  - [78] M.H. Nielsen, S. Aloni, J. De Yoreo, J. In situ TEM imaging of  $\text{CaCO}_3$  nucleation reveals coexistence of direct and indirect pathways, *Science* 345 (2014) 1158–1162.
  - [79] D. Potsma, Pyrite and siderite formation in brackish and freshwater swamp sediments, *Am. J. Sci.* 282 (1982) 1151–1183.
  - [80] A. Bernard, R.B. Symonds, The significance of siderite in the sediments from Lake Nyos, Cameroon, *J. Volcanol. Geotherm. Res.* 39 (1989) 187–194.
  - [81] T.L. Woods, R.M. Garrels, Calculated aqueous-solution-solid-solution relations in the low-temperature system  $\text{CaO-MgO-FeO-CO}_2\text{-H}_2\text{O}$ , *Geochem. Cosmochim. Acta* 56 (1992) 3031–3043.
  - [82] N.J. Tosca, I.A.M. Ahmed, B.M. Tutolo, A. Ashpitel, J.A. Hurowitz, Magnetite authigenesis and the warming of early Mars, *Nat. Geosci.* 11 (2018) 635.
  - [83] H.C.B. Hansen, *Environmental chemistry of iron (II)-iron (III) LDHs (green rusts)*, Nova Science Publishers, New York, 2001, pp. 413–434 Layer. Double Hydroxides: Present Future.
  - [84] B. Krapež, M.E. Barley, A.L. Pickard, Hydrothermal and resedimented origins of the precursor sediments to banded iron formation: sedimentological evidence from the Early Palaeoproterozoic Brockman Supersequence of Western Australia, *Sedimentology* 50 (2003) 979–1011.
  - [85] A.L. Pickard, M.E. Barley, B. Krapež, Deep-marine depositional setting of banded iron formation: sedimentological evidence from interbedded clastic sedimentary rocks in the early Palaeoproterozoic Dales Gorge Member of Western Australia, *Sediment. Geol.* 170 (2004) 37–62.
  - [86] L.R. Kump, W.E. Seyfried, Hydrothermal Fe fluxes during the Precambrian: effect of low oceanic sulfate concentrations and low hydrostatic pressure on the composition of black smokers, *Earth Planet. Sci. Lett.* 235 (2005) 654–662.
  - [87] W.E. Seyfried, K. Ding, The effect of redox on the relative solubilities of copper and iron in Cl-bearing aqueous fluids at elevated temperatures and pressures: an experimental study with application to seafloor hydrothermal systems, *Geochem. Cosmochim. Acta* 57 (1993) 1905–1917.
  - [88] W. Seyfried, K. Ding, M. Berndt, X. Chen, Experimental and theoretical controls on the composition of mid-ocean ridge hydrothermal fluids, *Volcanic Associated Massive Sulfide Deposits: Processes and Examples in Modern and Ancient Settings*, Economic Geology Publishing Company, 1997.
  - [89] K. Ding, W.E. Seyfried, Determination of Fe-Cl complexing in the low pressure supercritical region (NaCl fluid): iron solubility constraints on pH of seafloor hydrothermal fluids, *Geochem. Cosmochim. Acta* 56 (1992) 3681–3692.
  - [90] A.E. Isley, Hydrothermal plumes and the delivery of iron to banded iron formation, *J. Geol.* 169–185 (1995).
  - [91] D.R. Janecky, W.E. Seyfried, Formation of massive sulfide deposits on oceanic ridge crests: incremental reaction models for mixing between hydrothermal solutions and seawater, *Geochem. Cosmochim. Acta* 48 (1984) 2723–2738.
  - [92] M.K. Tivey, R.E. McDuff, Mineral precipitation in the walls of black smoker chimneys: a quantitative model of transport and chemical reaction, *J. Geophys. Res.* 95 (1990) 12617–12637.
  - [93] M.K. Tivey, The influence of hydrothermal fluid composition and advection rates on black smoker chimney mineralogy: insights from modeling transport and reaction, *Geochem. Cosmochim. Acta* 59 (1995) 1933–1949.
  - [94] J.C. Alt, Subseafloor processes in mid-ocean ridge hydrothermal systems, *Seafloor Hydrothermal Syst.: Phys. Chem. Biol. Geol. Interact.* 85–114 (1995).
  - [95] K. Von Damm, J. Bischoff, R. Rosenbauer, Quartz solubility in hydrothermal seawater: an experimental study and equation describing quartz solubility for up to 0.5 M NaCl solutions, *Am. J. Sci.* 291 (1991) 977–1007.
  - [96] R.A. Zierenberg, W.C. Shanks, W.E. Seyfried, R.A. Kosko, M.D. Strickler, Mineralization, alteration, and hydrothermal metamorphism of the ophiolite-hosted Turner-Albright sulfide deposit, southwestern Oregon, *J. Geophys. Res.: Solid Earth* 93 (1988) 4657–4674.
  - [97] N.J. Beukes, C. Klein, A.J. Kaufman, J.M. Hayes, Carbonate petrography, kerogen distribution, and carbon and oxygen isotope variations in an early Proterozoic transition from limestone to iron-formation deposition, Transvaal Supergroup, South Africa, *Econ. Geol.* 85 (1990) 663–690.
  - [98] O. Rouxel, N. Dobbek, J. Ludden, Y. Fouquet, Iron isotope fractionation during oceanic crust alteration, *Chem. Geol.* 202 (2003) 155–182.
  - [99] O. Rouxel, Y. Fouquet, J.N. Ludden, Subsurface processes at the Lucky Strike hydrothermal field, Mid-Atlantic ridge: evidence from sulfur, selenium, and iron isotopes, *Geochem. Cosmochim. Acta* 68 (2004) 2295–2311.
  - [100] H. Elderfield, A. Schultz, Mid-ocean ridge hydrothermal fluxes and the chemical composition of the ocean, *Annu. Rev. Earth Planet Sci.* 24 (1996) 191–224.
  - [101] D.J. Des Marais, When did photosynthesis emerge on earth? *Science* 289 (2000) 1703–1705.
  - [102] J. Korenaga, Archean geodynamics and the thermal evolution of earth, *Geophys. Monogr. Ser.* 164 (2006) 7–32.
  - [103] D.A. Kulik, M.N. Korzhnev, Lithological and geochemical evidence of Fe and Mn pathways during deposition of Lower Proterozoic banded iron formation in the Krivoy Rog Basin (Ukraine), *Geol. Soc. Lond. Special Publ.* 119 (1997) 43–80.
  - [104] C. Klein, N.J. Beukes, Geochemistry and sedimentology of a facies transition from limestone to iron-formation deposition in the early Proterozoic Transvaal Supergroup, South Africa, *Econ. Geol.* 84 (1989) 1733–1774.
  - [105] A.J. Kaufman, J.M. Hayes, C. Klein, Primary and diagenetic controls of isotopic compositions of iron-formation carbonates, *Geochem. Cosmochim. Acta* 54 (1990) 3461–3473.
  - [106] D.Y. Sumner, Carbonate precipitation and oxygen stratification in late Archean seawater as deduced from facies and stratigraphy of the Gamohaan and Frisco formations, Transvaal Supergroup, South Africa, *Am. J. Sci.* 297 (1997) 455–487.
  - [107] N.J. Beukes, Sedimentology of the Kuruman and Griquatown iron-formations, Transvaal supergroup, Griqualand west, South Africa, *Precambrian Res.* 24 (1984) 47–84.
  - [108] W. Stumm, *Chemistry of the Solid-Water Interface: Processes at the Mineral-Water and Particle-Water Interface in Natural Systems*, John Wiley & Son Inc., 1992.
  - [109] C.I. Steefel, P. Van Cappellen, A new kinetic approach to modeling water-rock interaction: the role of nucleation, precursors, and Ostwald ripening, *Geochem. Cosmochim. Acta* 54 (1990) 2657–2677.
  - [110] A.E. Nielsen, O. Söhnel, Interfacial tensions: electrolyte crystal-aqueous solution, from nucleation data, *J. Cryst. Growth* 11 (1971) 233–242.
  - [111] M.L. Johnson, *Ferrous Carbonate Precipitation Kinetics-A Temperature Ramped Approach*, Ph. D. Thesis, Rice University, Houston, Texas, 1991.

- [112] C. Jimenez-Lopez, C.S. Romanek, Precipitation kinetics and carbon isotope partitioning of inorganic siderite at 25° C and 1 atm 1, *Geochem. Cosmochim. Acta* 68 (2004) 557–571.
- [113] T.F. Bristow, R.M. Haberle, D.F. Blake, D.J. Des Marais, J.L. Eigenbrode, A.G. Fairén, J.P. Grotzinger, K.M. Stack, M.A. Mischna, E.B. Rampe, K.L. Siebach, B. Sutter, D.T. Vaniman, A.R. Vasavada, Low Hesperian pCO<sub>2</sub> constrained from *in situ* mineralogical analysis at Gale Crater, Mars, *Proc. Natl. Acad. Sci. U. S. A.* 114 (2017) 201616649.
- [114] C.B. Field, M.J. Behrenfeld, J.T. Randerson, P. Falkowski, Primary production of the biosphere: integrating Terrestrial and oceanic components, *Science* 237–239 (1998).
- [115] R. Siever, Silica solubility, 0–200°C, and the diagenesis of siliceous sediments, *J. Geol.* 127–150 (1962).
- [116] W. Feitknecht, P. Schindler, Solubility constants of metal oxides, metal hydroxides and metal hydroxide salts in aqueous solution, *Pure Appl. Chem.* 6 (1963) 125–206.
- [117] P.C. Singer, W. Stumm, Acid mine drainage - the rate determining step, *Science* 167 (1970) 1121–1123.
- [118] J.D. Rimstidt, Quartz solubility at low temperatures, *Geochem. Cosmochim. Acta* 61 (1997) 2553–2553.
- [119] D.R. Janecky, W.E. Seyfried, Formation of massive sulfide deposits on oceanic ridge crests: incremental reaction models for mixing between hydrothermal solutions and seawater, *Geochem. Cosmochim. Acta* 48 (1984) 2723–2738.
- [120] J.W. Johnson, E.H. Oelkers, H.C. Helgeson, SUPCRT92: a software package for calculating the standard molal thermodynamic properties of minerals, gases, aqueous species, and reactions from 1 to 5000 bar and 0 to 1000 deg C, *Comput. Geosci.* 18 (1992) 899–947.
- [121] X.Z. Kong, B.M. Tutolo, Saar M.O. DBCreate, A SUPCRT92-based program for producing EQ3/6, TOUGHREACT, and GWB thermodynamic databases at user-defined T and P, *Comput. Geosci.* 51 (2013) 415–417.
- [122] C. Klein, Greenalite, stilpnomelane, minnesotaite, crocidolite and carbonates in a very low-grade metamorphic Precambrian iron formation, *Can. Mineral.* 12 (1974) 475–498.
- [123] M.G. Rasmussen, B.W. Evans, S.M. Kuehner, Low-temperature fayalite, greenalite, and minnesotaite from the Overlook gold deposit, Washington; phase relations in the system FeO-SiO<sub>2</sub>-H<sub>2</sub>O, *Can. Mineral.* 36 (1998) 147–162.
- [124] C.I. Steefel, P. Van Cappellen, A new kinetic approach to modeling water-rock interaction: the role of nucleation, precursors, and Ostwald ripening, *Geochem. Cosmochim. Acta* 54 (1990) 2657–2677.